www.nature.com/mi

MucosalImmunology

ARTICLE

Entamoeba histolytica exploits the autophagy pathway in macrophages to trigger inflammation in disease pathogenesis

Sharmin Begum[1], France Moreau[1], Antoine Dufour[2,3] and Kris Chadee[1]

The mechanism whereby *Entamoeba histolytica* (*Eh*) binding with macrophages at the intercellular junction triggers aggressive pro-inflammatory responses in disease pathogenesis is not well understood. The host intracellular protein degradation process autophagy and its regulatory proteins are involved in maintenance of cellular homeostasis and excessive inflammatory responses. In this study we unraveled how *Eh* hijacks the autophagy process in macrophages to dysregulate pro-inflammatory responses. Direct contact of live *Eh* with macrophages activated caspase-6 that induced rapid proteolytic degradation of the autophagy ATG16L1 protein complex independent of NLRP3 inflammasome and caspase-3/8 activation. Crohn's disease susceptible ATG16L1 T300A variant was highly susceptible to *Eh*-mediated degradation that augmented pro-inflammatory cytokines in mice. Quantitative proteomics revealed downregulation of autophagy and vesicle-mediated transport and upregulation of cysteine-type endopeptidase pathways in response to *Eh*. We conclude during *Eh*-macrophage outside-in signaling, ATG16L1 protein complex plays an overlooked regulatory role in shaping the pro-inflammatory landscape in amebiasis.

Mucosal Immunology (2021) 14:1038–1054; https://doi.org/10.1038/s41385-021-00408-4

INTRODUCTION

A unique feature of *Eh* infection is its ability to remain asymptomatic in ≥90% of cases and only a limited subset of infected individuals (≤10%) develop disease symptoms.[1] The underlying explanation for intermittent symptomatic infection is not fully understood but appear to be dependent on the host immune regulatory system, genetics, and potency of immune responses. As *Eh* is too large (range 10–60 µm) to be phagocytized by neutrophils and macrophages, the host innate immune system needs to recognize and respond to the presence of invasive *Eh*.[2] Direct interaction of *Eh* with host cells is the first critical step that shapes the outcome of infection. This interaction is primarily mediated by *Eh* surface adhesin, the Gal/GalNAc lectin (Gal-lectin), which delivers an intercellular "adhesive" signal to the contacted cell.[3] Inhibition of *Eh* Gal-lectin mediated binding with exogenous D-galactose blocks intercellular interactions and subsequent pro-inflammatory responses.[3,4] Along with surface Gal-lectin, the *Eh* genome encodes numerous genes for cysteine proteases (CPs) that play major roles in *Eh* virulence and invasiveness.[5,6] In addition, the immune response elicited by host cells following *Eh* contact is a key determinant of host susceptibility to develop disease. *Eh* interaction with macrophages triggers elevated pro-inflammatory cytokine TNF-α secretion[7] and activation of different caspases, a group of proteolytic enzymes required for homeostasis through the regulation of cell death and inflammation.[8] We have shown that direct *Eh* contact with macrophages via the Gal-lectin provides a platform to engage *Eh* cysteine protease 5 (*Eh*CP-A5) RGD sequence with macrophage $\alpha_5\beta_1$ integrin for NLRP3 inflammasome activation of caspase-1 that cleaves intracellular pro IL-1β and IL-18 into their active forms.[2,9] Similarly, *Eh* Gal-lectin and *Eh*CP-A5 mediated interaction with macrophages induced caspase-4 activation, which function upstream of caspase-1 to enhance the cleavage of caspase-1 CARD domain and both caspases degrade the membrane pore forming protein gasdermin D to facilitate IL-1β secretion.[10] Another cellular mechanism following *Eh*-macrophage contact involves *Eh*CP-A1 and *Eh*CP-A4 induced caspase-6 activation, which degrades cytoskeletal-associated proteins to trigger IL-1β secretion from macrophages.[11]

The innate immune system triggered inflammation is a double-edged sword: it can protect the host from invasive *Eh* infection or it can promote severe tissue damage that facilitates *Eh* dissemination. Human intestinal xenografts treated with antisense oligonucleotide against p65 subunit of NF-κB before *Eh* inoculation, showed significant reduction in pro-inflammatory cytokine secretion and reduced tissue damage compared to control xenografts.[12] To regulate excessive inflammatory responses, the host intracellular degradation process autophagy and autophagy-associated proteins play important roles.[13] In autophagy process, portions of cytoplasm and damaged organelles are sequestered into a double-membrane vesicle known as autophagosome and subsequently undergo fusion with the lysosome for the break-down and recycling of their content.[14] Loss of autophagy or deficiency of autophagy protein ATG16L1 in macrophages significantly increases IL-1β and IL-18 production in response to lipopolysaccharide (LPS), ATP, or monosodium urate crystals.[15] Mice with ATG16L1 deficient hematopoietic cells or expressing Crohn's disease associated ATG16L1 T300A variant are susceptible to develop colitis due to proteolytic cleavage by caspase-3.[16–18] As autophagy and autophagy-associated proteins can limit inflammation and interruption in autophagy enhances NLRP3-inflammasome dependent cytokine production,[19] *Eh*-macrophage interactions was used as a model to interrogate this interplay. We

[1]Departments of Microbiology, Immunology and Infectious Diseases, Calgary, AB, Canada; [2]Physiology and Pharmacology, Snyder Institute for Chronic Diseases, University of Calgary, Calgary, AB, Canada and [3]Biochemistry and Molecular Biology, Snyder Institute for Chronic Diseases, University of Calgary, Calgary, AB, Canada
Correspondence: Kris Chadee (kchadee@ucalgary.ca)

Received: 23 December 2020 Revised: 25 March 2021 Accepted: 16 April 2021
Published online: 7 May 2021

hypothesize that the outcome of infection is determined at the *Eh*-macrophage intercellular junction that subsequently alter host regulatory processes.

In this study, we found that constitutively expressed intact ATG16L1 protein complex was rapidly degraded by caspase-6 proteolytic activity in macrophage following contact with live *Eh* via Gal-lectin and *Eh*CP-A1 and *Eh*CP-A4 at the intercellular junction. Intriguingly, we identified that the ATG16L1 protein is a novel substrate for caspase-6 degradation that enhanced pro-inflammatory cytokine responses. Global proteome analysis of *Eh*-macrophage interaction revealed downregulation of autophagy and vesicle-mediated transport pathways and upregulation of cysteine-type endopeptidase activity. This study illuminates that *Eh* outside-in signaling at the macrophage intercellular junction is a critical first step in mediating caspase-6 dependent ATG16L1 protein complex degradation that controls pro-inflammatory cytokine release in *Eh* disease pathogenesis.

RESULTS

Eh induces degradation of the autophagy-associated ATG16L1 protein complex

The intracellular protein degradation system autophagy negatively regulates inflammasome activation and loss of autophagy ATG16L1 protein increases caspase-1 activation with elevated IL-1β and IL-18 production by endotoxin.[15,20–22] We investigated whether autophagy proteins were altered during *Eh* interaction as NLRP3 inflammasome recruitment with caspase-1 activation and high IL-1β secretion is well characterized during *Eh*-macrophage contact.[2] Surprisingly, we observed that intact ATG16L1 protein in human macrophages undergoes rapid degradation in response to *Eh* in a time- and dose-dependent manner (Fig. 1a, b). Within 5 min of *Eh*-macrophage interaction, full length ATG16L1 protein (66/68 kDa) was degraded into multiple fragments (43 and 25 kDa) as compared to basal negative controls (Fig. 1a). Complete degradation of ATG16L1 protein was observed within 10 min (Fig. 1a) and with high *Eh*-macrophage ratios (1:5–1:20); degradation was not detected with the lowest *Eh*-macrophage ratio (1:80; Fig. 1b). Mouse bone marrow derived macrophages (BMDMs; Fig. 1c, d) and human colonic T84 epithelial cells (Supplementary Fig. S1a, b) showed similar time- and dose-dependent degradation of ATG16L1 protein in response to *Eh*.

ATG16L1 protein forms a multimeric complex with ATG12-ATG5 conjugate, which is essential for the conversion of LC3–1 to phosphatidylethanolamine (PE) conjugated LC3–2 form.[23] Thus, we sought to investigate the ATG12-ATG5 conjugate after *Eh* interaction with macrophages and observed a time-dependent dissociation of ATG5 protein from the conjugate as compared to basal untreated cells (Fig. 1a, c). Similar to ATG16L1 protein degradation, there was a dose-dependent ATG5 protein dissociation, highest with 1:5–1:20 and no effect with 1:80 *Eh*-macrophage ratio (Fig. 1b, d). ATG16L1 is an ATG5-binding protein[24] thus, rapid degradation of ATG16L1 might be the cause for ATG5 dissociation. By immunostaining of the ATG16L1 protein basally and in response to *Eh* stimulation in macrophages via confocal microscopy, we observed significant reduction (~50%) in ATG16L1 cytoplasmic staining upon interaction with *Eh* (Fig. 1e, f). To discern the contribution of *Eh*-triggered NLRP3 inflammasome activation, *Nlrp3*$^{-/-}$ and *Asc*$^{-/-}$ BMDM were stimulated with *Eh* and observed a similar trend of ATG16L1 protein degradation as WT BMDM (Supplementary Fig. S1c, d). We also determine LC3–1 to LC3–2 conversion in response to *Eh* stimulation from 2 to 40 min and did not observe any reduction in LC3–2 (Supplementary Fig. S1e). When we compared *Eh*-stimulated LC3–2 levels at 5 and 10 min with the known autophagy inducer, Torin (mTOR inhibitor) and Bafilomycin A1 (inhibitor of autophagosome-lysosome fusion), there was also no change in LC3–2 levels (Supplementary Fig. S1f). The absence of LC3–1/LC3–2 levels was possibly due to the early time points of stimulation with *Eh* and the existence of continuous homeostatic process of autophagy within the cell for turn over. As LC3–1/LC3–2 conversion is the final step of the autophagy process as compared to ATG16L1 complex formation, this could be another reason for not observing any change in LC3–1/LC3–2 levels. These results demonstrate that *Eh*-macrophage interaction triggers alteration of autophagy-associated ATG16L1 protein complex by inducing its degradation and dissociation of ATG5 from ATG12-ATG5 conjugate, which are independent of the NLRP3 inflammasome recruitment and activation.

Live *Eh* facilitate direct contact and cysteine protease dependent ATG16L1 protein degradation

To investigate the necessity of *Eh* surface Gal-lectin mediated adherence in ATG16L1 protein degradation, exogenous galactose was used to competitively inhibit *Eh*-macrophage interaction.[4] Exogenous galactose completely inhibited ATG16L1 protein degradation and ATG5 dissociation from ATG12-ATG5 conjugate as compared to *Eh* only treatment (Fig. 2a). Based on these findings, we investigated whether stimulation with different subcellular fractions of *Eh* or soluble native Gal-lectin could trigger ATG16L1 protein degradation in macrophages. As predicted, only live *Eh*-induced ATG16L1 protein degradation along with ATG5 dissociation (Fig. 2b) but not with *Eh* secreted proteins (50 µg), whole lysates of *Eh* (WL), or with cytoplasmic (CM) or membrane (MM) fractions or soluble native Gal-lectin (Fig. 2b, c). These observations demonstrate that surface Gal-lectin mediated contact of live *Eh* with macrophages is required to induce ATG16L1 protein degradation along with the involvement of other *Eh* surface molecules as observed in our earlier studies.[2,10,11]

To investigate if other well-characterized *Eh* virulent factors such as CPs played a role in ATG16L1 protein degradation, live *Eh* were pre-treated overnight with the irreversible CP inhibitor, E-64 that prevented ATG16L1 protein degradation (Fig. 2d). These results demonstrate that following Gal-lectin mediated contact with macrophages, *Eh*CPs are involved in ATG16L1 protein degradation. We have previously shown that surface *Eh*CP-A5 degrades MUC2 mucin and binds macrophage integrins to activate inflammasome.[2,5,25] To determine the role of *Eh*CP-A5, macrophages were stimulated with *Eh*CP-A5 deficient parasites and similar ATG16L1 protein degradation was observed as wild type *Eh*, whereas E-64 treated *Eh* completely inhibited degradation (Fig. 2e). We have recently shown that following *Eh*-macrophage interaction, *Eh*CP-A1 and *Eh*CP-A4 are recruited to the intercellular junction that facilitated the degradation of cytoskeletal-associated proteins.[11] *Eh*CP-A1 is involved in *Eh* invasion in human intestinal xenografts in SCID mice[26] and *Eh*CP-A4 is the most upregulated CPs during *Eh* cecal infection in mice.[27] To explore whether these two proteases played a role in ATG16L1 degradation, *Eh* were pre-treated with specific inhibitors for *Eh*CP-A1 (WRR483) and *Eh*CP-A4 (WRR605) separately, or both in combination before incubation with macrophages. Individually, *Eh*CP-A1 and *Eh*CP-A4 inhibitors partially restrained ATG16L1 protein degradation whereas, pre-treatment in combination, completely rescued ATG16L1 from degradation (Fig. 2f). Similar effects were observed in BMDM treated with E-64, *Eh*CP-A1 (WRR483), and *Eh*CP-A4 (WRR605) inhibitors alone or in combination that restored ATG16L1 protein degradation (Fig. 2g). These results suggest that at the intercellular junction between live *Eh*-macrophage, along with Gal-lectin contact both *Eh*CP-A1 and *Eh*CP-A4 assisted in ATG16L1 protein degradation.

Eh-induced caspase-6 activation mediates ATG16L1 protein degradation

In eukaryotic cells, protein degradation is mainly mediated by the ubiquitin-proteasome pathway. To investigate the involvement of the proteasome pathway in ATG16L1 degradation, macrophages

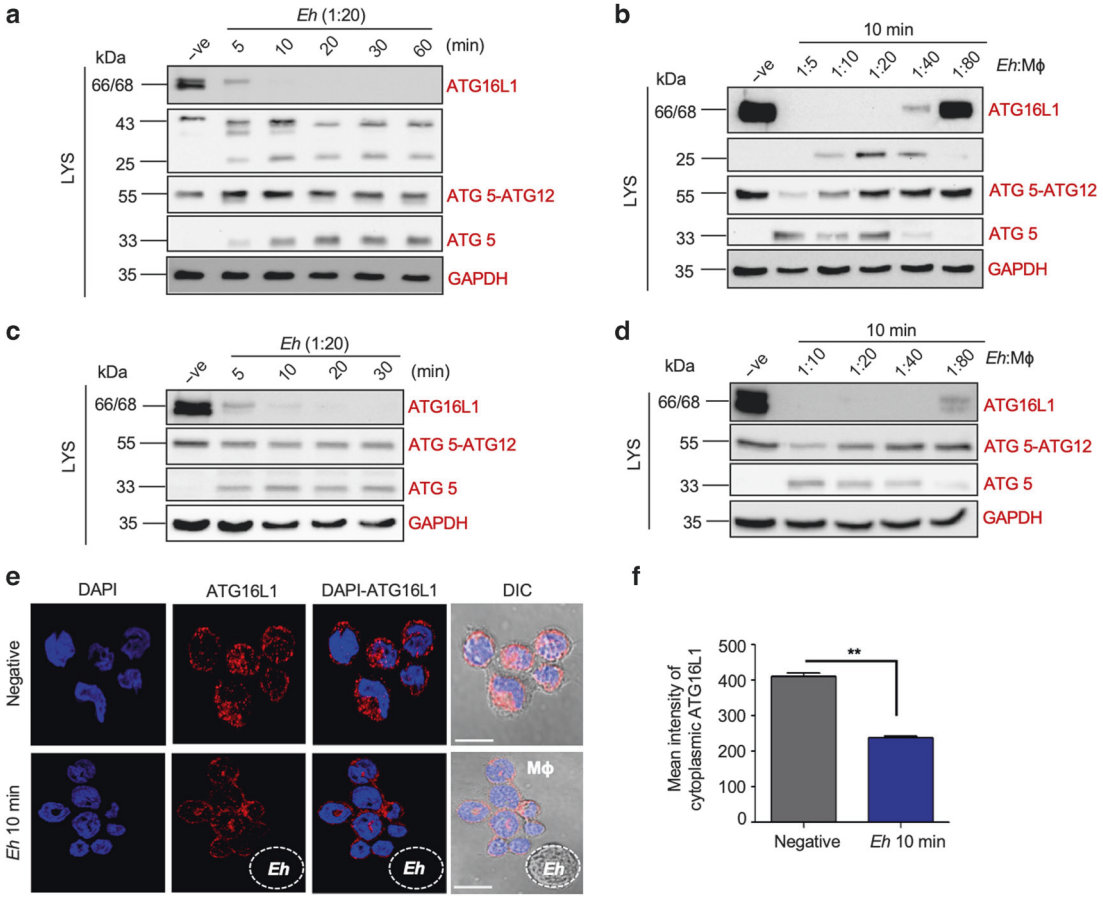

Fig. 1 *Eh* induces ATG16L1 protein complex degradation. *Eh*-induced ATG16L1 degradation and dissociation of ATG5 protein from ATG12-ATG5 conjugate were revealed in THP-1 macrophages stimulated with **a**, different time point with *Eh* at 1:20 ratio **b**, different *Eh* to macrophage ratio for 10 min. Bone marrow derived macrophages (BMDMs) were stimulated with **c**, different time points with *Eh* at 1:20 ratio **d**, for different *Eh* to macrophage ratio for 10 min. **e** THP-1 macrophages were stimulated with for 10 min and cytoplasmic immunostaining of ATG16L1 proteins were observed by confocal microscopy. Representative images of control and *Eh* interacted macrophages (MΦ) from three independent experiments (scale bar 10 μm). **f** Measurement of cytoplasmic mean intensity of ATG16L1 protein at the basal level and after *Eh* stimulation was shown as mean ± SEM. Mean fluorescence intensity was measured from 7/8 images from three independent experiments. Cells without any treatment is symbolized as (−ve). Statistical significance was determined by *t*-test. $^{**}P < 0.01$. Results are representative of three independent experiments ($n = 3$).

were pre-treated with MG132 (proteasome inhibitor) and ALLN (calpain I/II, cathepsin B and proteasome inhibitor) followed by *Eh* stimulation. Inhibition with these proteasome pathway inhibitors were not able to rescue ATG16L1 degradation compared to only *Eh* stimulation (Supplementary Fig. S2a, b). Human and murine ATG16L1 proteins are susceptible to cleavage by a caspase-dependent manner during apoptosis induced by death-receptor stimulation or by staurosporine (STS).[16] As *Eh* activates several caspases upon contact with macrophages,[2,10,11] we next explored whether ATG16L1 protein degradation was mediated by the proteolytic activity of caspases. To address this, macrophages were pre-treated with the pan-caspase inhibitor Z-VAD-fmk and following stimulation with *Eh*, ATG16L1 protein degradation was completely inhibited in a dose-dependent manner (Fig. 3a). To ascertain the involvement of specific caspases, we tested CASP1 and CASP4 CRISPR/Cas9 KO THP-1 macrophages in comparison with WT THP-1 (Supplementary Fig. S2c) and with specific inhibitors for caspase-3 (Z-DEVD-fmk), -8 (Z-IETD-fmk) (Supplementary Fig. S2d), and -6 (Z-VEID-fmk) (Fig. 3b). Except for the caspase-6 inhibitor Z-VEID-fmk, none of the other inhibitors and CRISPR/Cas9 KO cells were able to restore ATG16L1 protein degradation (Fig. 3b). Caspase-6 specific inhibitor Z-VEID-fmk dose-dependently restored ATG16L1 protein degradation and inhibited ATG5 dissociation from the ATG12-ATG5 conjugate (Fig. 3b). As a control for caspase-6 inhibition, restitution of caspase-6 pro-form and its substrate lamin A/C was observed upon *Eh* stimulation (Fig. 3b). As expected, *Eh* in contact with macrophages triggered time-dependent appearance of the active caspase-6 fragment (18-kDa) along with degradation of its specific substrate lamin A/C (Fig. 3c). Caspase-6 enzymatic activity assay showed that upon *Eh* stimulation in the presence or absence of the caspase-6 inhibitor Z-VEID-fmk, there was a significant time-dependent increase in caspase-6 activity compared to Z-VEID-fmk treated and negative control cells (Fig. 3d). Similar restoration of ATG16L1 along with inhibition of ATG5 dissociation were observed in BMDMs in presence or absence of Z-VAD-fmk pan-caspase and Z-VEID-fmk caspase-6 inhibitor (Fig. 3e). To further validate the role of caspase-6 in ATG16L1 protein degradation, caspase-6 was silenced in vitro by siRNA, and following *Eh* stimulation both ATG16L1 and lamin A/C protein degradation were inhibited in caspase-6 silenced cells compared to the scramble siRNA control (Fig. 3f).

To explore the probable mechanism of *Eh*-induced caspase-6 activation, we have previously reported dynamic cytoskeleton rearrangement in macrophages upon interaction with *Eh* at the intercellular junction.[11] Similarly, we also observed actin and tubulin polarization towards the *Eh*-macrophage contact site (white arrows) as compared to non-contacted cells

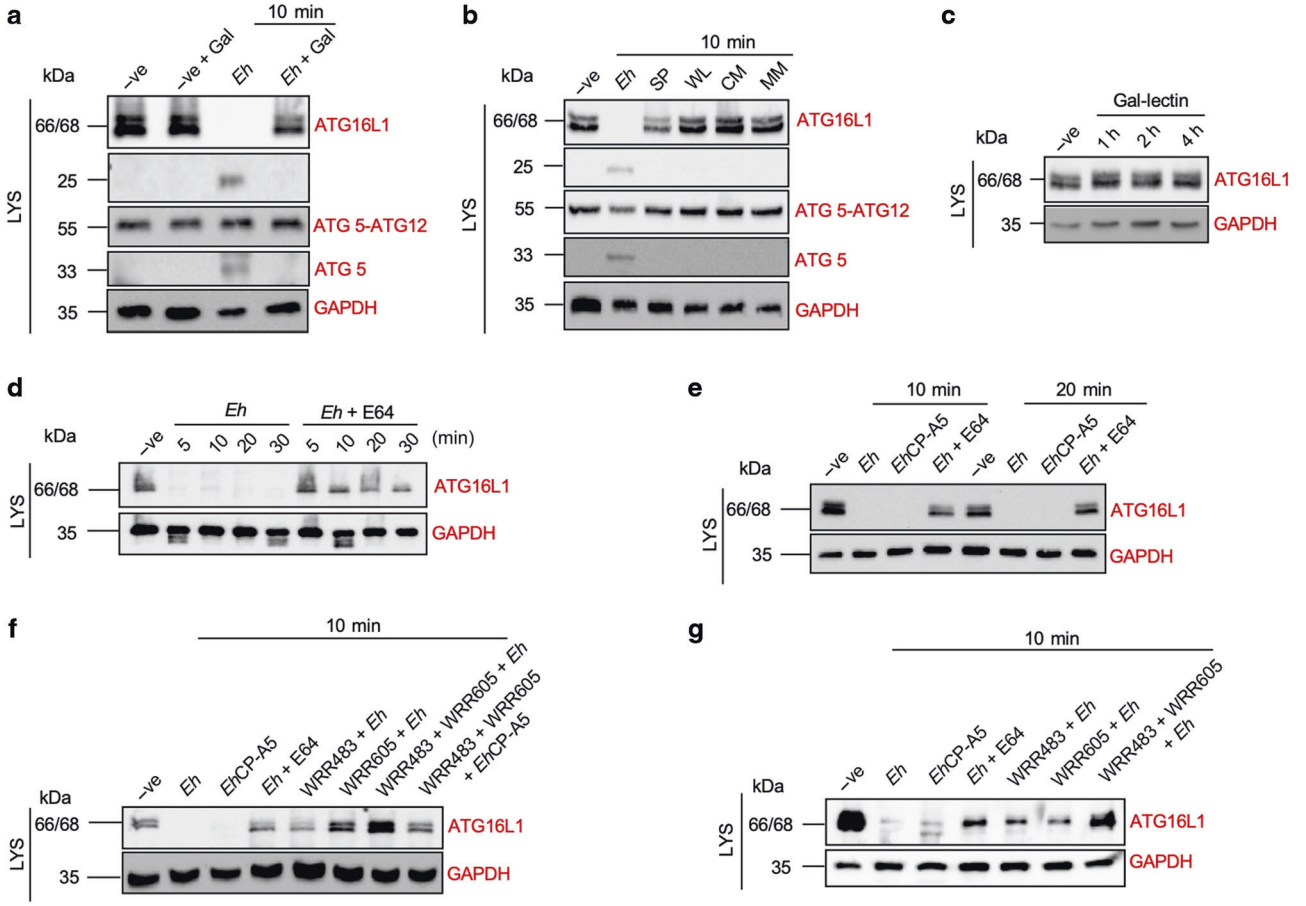

Fig. 2 Direct contact of live *Eh* via Gal-lectin and *Eh*CP-A1/*Eh*CP-A4 mediates ATG16L1 protein degradation. a *Eh* were pre-treated with 55 mM galactose for 5 min before incubation with THP-1 macrophages for 10 min at 1:20 ratio. **b** THP-1 macrophages were stimulated with live *Eh* (1:20 ratio), *Eh* secreted proteins (SP, 50 μg), *Eh* whole lysate (WL), *Eh* cytoplasmic component (CM), and *Eh* membrane component prepared from equivalent amount of *Eh* for 10 min. **c** THP-1 macrophages were incubated with native Gal-lectin (500 ng/ml) for increasing times. **d** *Eh* were pre-treated overnight with E-64 (100 μM) and incubated with macrophages for different time points along with non-treated *Eh*. **e** THP-1 macrophages were stimulated with wild type *Eh*, *Eh*CP-A5 deficient *Eh*, and E-64 treated *Eh* for 10 min and 20 min. *Eh* were also pre-treated with specific inhibitor for EhCP-A1 (WRR483, 20 μM), EhCP-A4 (WRR605, 20 μM) individually or both together and incubated with (**f**) THP-1 and (**g**) bone marrow derived macrophages (BMDMs) for 10 mins. Equal amount of lysed cell lysates was loaded onto SDS-PAGE gel and immunoblotted with indicated antibodies. Cells without treatment is symbolized as (−ve). *Eh*-macrophage 1:20 ratio used. Results are representative of three independent experiments ($n = 3$).

(Supplementary Fig. S3a). To characterize the role of actin rearrangement in caspase-6 activation, macrophages were pre-treated with cytochalasin D (inhibitor of actin polymerization) and stimulated with *Eh* for 10 min. As expected, due to inhibition of actin polymerization there was no ATG16L1 degradation or active caspase-6 (Supplementary Fig. S3b). To illustrate the role of *Eh*CP-A1 and *Eh*CP-A4 in caspase-6 activation, macrophages were stimulated with WT *Eh*, *Eh*CP-A5 deficient parasites and WT *Eh* pre-treated with various CP inhibitors (E-64, WRR483 for *Eh*CP-A1, WRR605 for *Eh*CP-A4 or WRR483 and WRR605 together). In accordance with our earlier results (Fig. 2f, g), caspase-6 was not activated in the presence of E-64, WRR483, WRR605 or with WRR483 and WRR605 together as compared to the WT and *Eh*CP-A5 deficient parasites (Supplementary Fig. S3c).

Caspase-3/-8 independent ATG16L1 degradation elicits pro-inflammatory cytokines in response to *Eh*

In response to *Eh*, while active caspase-6 mediates ATG16L1 protein degradation, activation of caspase-6 can be mediated by caspase-3 or by autoactivation.[28–30] To investigate whether caspase-3 was activated in response to *Eh*, macrophages were examined up to 30 min stimulation and showed no caspase-3 activation as compared to the positive control, STS (Fig. 4a). In addition, macrophages were pre-treated with caspase-6 and caspase-3 specific inhibitors (Z-VEID-fmk and Z-DEVD-fmk, respectively) to compare ATG16L1 degradation in response to *Eh*. As predicted, Z-VEID-fmk restored ATG16L1 degradation whereas Z-DEVD-fmk did not (Fig. 4b). Consistent with this, caspase-6 substrate lamin A/C was restored in the presence of Z-VEID-fmk but not with Z-DEVD-fmk (Fig. 4b). Similar results were observed with BMDMs, where pre-treatment with Z-DEVD-fmk was not able to restore ATG16L1 degradation (Fig. 4c). These results suggest that in response to *Eh*, ATG16L1 protein degradation was mediated by caspase-6 independent of caspase-3 activation. Protein-protein interaction networking by STRING v11 (https://string-db.org) showed that apart from caspase-3, caspase-8 is highly interacted with caspase-6 (Supplementary Fig. S4a), however, inhibition of caspase-8 with its specific inhibitor Z-IETD-fmk, had no effect on ATG16L1 degradation in response to *Eh* (Fig. 4c).

ATG16L1 is essential for suppression of endotoxin-induced intestinal inflammatory responses as loss of ATG16L1 has been shown to be associated with high IL-1β and IL-18 production.[15] In response to *Eh*, ATG16L1 degradation potentiated pro-inflammatory cytokine TNF-α expression and IL-1β and IL-18 production along with caspase-1 activation, which were diminished due to ATG16L1 restoration by Z-VEID-fmk treatment

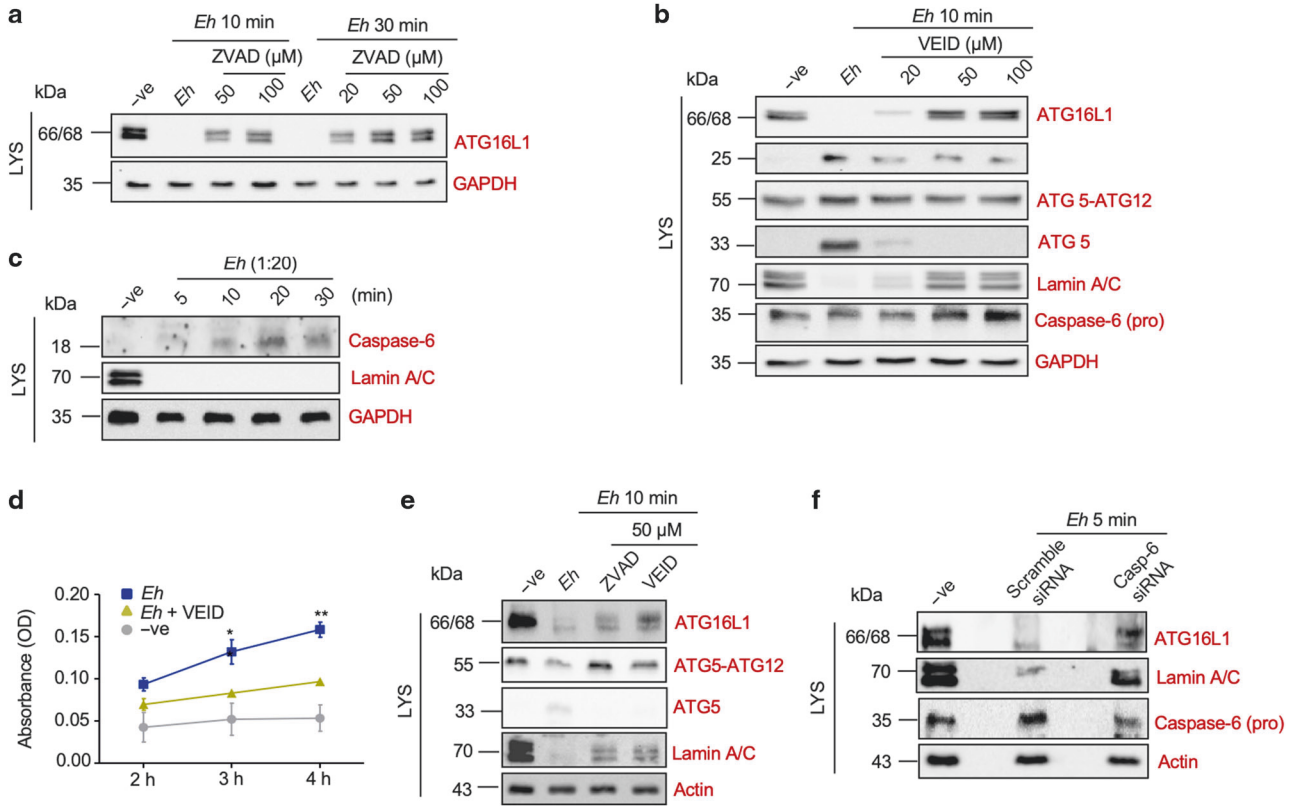

Fig. 3 ***Eh*-induced active caspase-6 mediated ATG16L1 protein degradation. a** THP-1 macrophages were pre-treated with pan-caspase inhibitor Z-VAD-fmk (50, 100 μM) for 1 h before incubation with *Eh* for 10 and 30 min. **b** THP-1 macrophages were pre-treated with caspase-6 inhibitor Z-VEID-fmk (20, 50, 100 μM) for 1 h before stimulation with *Eh* for 10 min. **c** THP-1 macrophages were stimulated with *Eh* for different time points to detect active caspase-6 and its known substrate lamin A/C. **d** Caspase-6 activity was measured in presence of *Eh* and *Eh* along with caspase-6 inhibitor Z-VEID-fmk (50 μM). **e** Bone marrow derived macrophages (BMDMs) were pre-treated with pan-caspase inhibitor Z-VAD-fmk and caspase-6 inhibitor Z-VEID-fmk for 1 h with 50 μM concentration prior to stimulation with *Eh* for 10 min. Restoration of ATG16L1 protein and ATG12-ATG5 conjugate were assessed by western blot along with lamin A/C restoration. **f** THP-1 macrophages were transfected with 50 nM caspase-6 siRNA, or scramble siRNA by nuclear factor technique. After 48 h, transfected cells were stimulated with *Eh* for 5 min and western blot was performed to detect indicated proteins. Equal amount of lysed cell lysates was loaded onto SDS-PAGE gel and immunoblotted with indicated antibodies. Cells without any treatment is symbolized as (−ve). *Eh*-macrophage 1:20 ratio used. Results are representative of three independent experiments ($n = 3$). $^{*}P < 0.05$, $^{**}P < 0.01$.

(Fig. 4d, e). These results demonstrate that intact ATG16L1 is a necessary component to control *Eh*-induced pro-inflammatory responses. To elucidate a role for intact ATG16L1 in intestinal amebiasis, we performed a short-term mouse colonic loop study with *Eh*.[31] After 3 h *Eh* inoculation in the proximal colon, ATG16L1 degradation was significantly increased as compared to control tissues (Fig. 4f). ATG16L1 degradation correlated with significantly increased pro-inflammatory cytokines (TNF-α, IL-1β) and chemokines (MCP-1, KC) expression in *Eh* inoculated loops (Fig. 4g). A similar increase was observed in BMDM stimulated with *Eh*, for TNF-α, IL-1β, MCP-1, KC (Fig. 4h) and other cytokines (Supplementary Fig. S4b).

WT and ATG16L1 T300A variant susceptibility towards *Eh*

A single nucleotide polymorphism (SNP) in the ATG16L1 (T300A in human, T316A in mice) gene is associated with increased susceptibility for Crohn's disease, presence of defective Paneth cell and goblet cell morphology and enhanced sensitization for caspase-3 mediated degradation.[16] As caspase-3 activation was not observed in this study upon *Eh*-macrophage interaction, we tested the effect of *Eh* on the ATG16L1 T316A variant. BMDM cells from WT and ATG16L1 T316A variant were stimulated with different time points and *Eh*-macrophage ratios. Both ATG16L1 WT and ATG16L1 T316A variant were rapidly degraded (Supplementary Fig. S5a) but surprisingly, using different *Eh*-macrophage ratios revealed that the ATG16L1 T316A variant was highly susceptible of *Eh*-induced degradation at 1:80 ratio as compared to WT ATG16L1 (highlighted Fig. 5a). We used the caspase-6 inhibitor Z-VEID-fmk in WT and ATG16L1 T316A variant BMDM to restore ATG16L1 degradation and as expected, in WT BMDM ATG16L1 restored efficiently but the ATG16L1 T316A variant showed more sensitivity to *Eh*-induced degradation in the presence of Z-VEID-fmk (Supplementary Fig. S5b). These results confirm the high susceptibility of the ATG16L1 T316A variant to degradation in response to *Eh*. The partial restoration of ATG16L1 T316A variant might be due to its high sensitivity towards caspase-3, though we did not observe caspase-3 activation in response to *Eh*. Next, to ascertain the efficiency of active caspase-6 mediated ATG16L1 degradation, we quantified the cleavage of WT and ATG16L1 T300A variant in transfected HEK293T cells. Both WT and ATG16L1 T300A variant proteins were degraded with recombinant CASP-6 (rCASP-6) that was restored in the presence of Z-VEID-fmk. However, the T300A variant showed increased susceptibility for degradation with more degraded fragments as compared to ATG16L1 WT (Fig. 5b). We next interrogated if the ATG16L1 T316A variant mice were more susceptible to *Eh*-induced pro-inflammatory responses in colonic loop studies after 3 h inoculation. As predicted, the ATG16L1 T316A variant mice showed enhanced pro-inflammatory IL-1β and IL-6 mRNA (Fig. 5c) and chemokine KC and MCP-1 expression (Fig. 5d) as compared to ATG16L1 WT controls. Myeloperoxidase (MPO) activity in WT and ATG16L1 T316A variant mice after *Eh* inoculation showed an

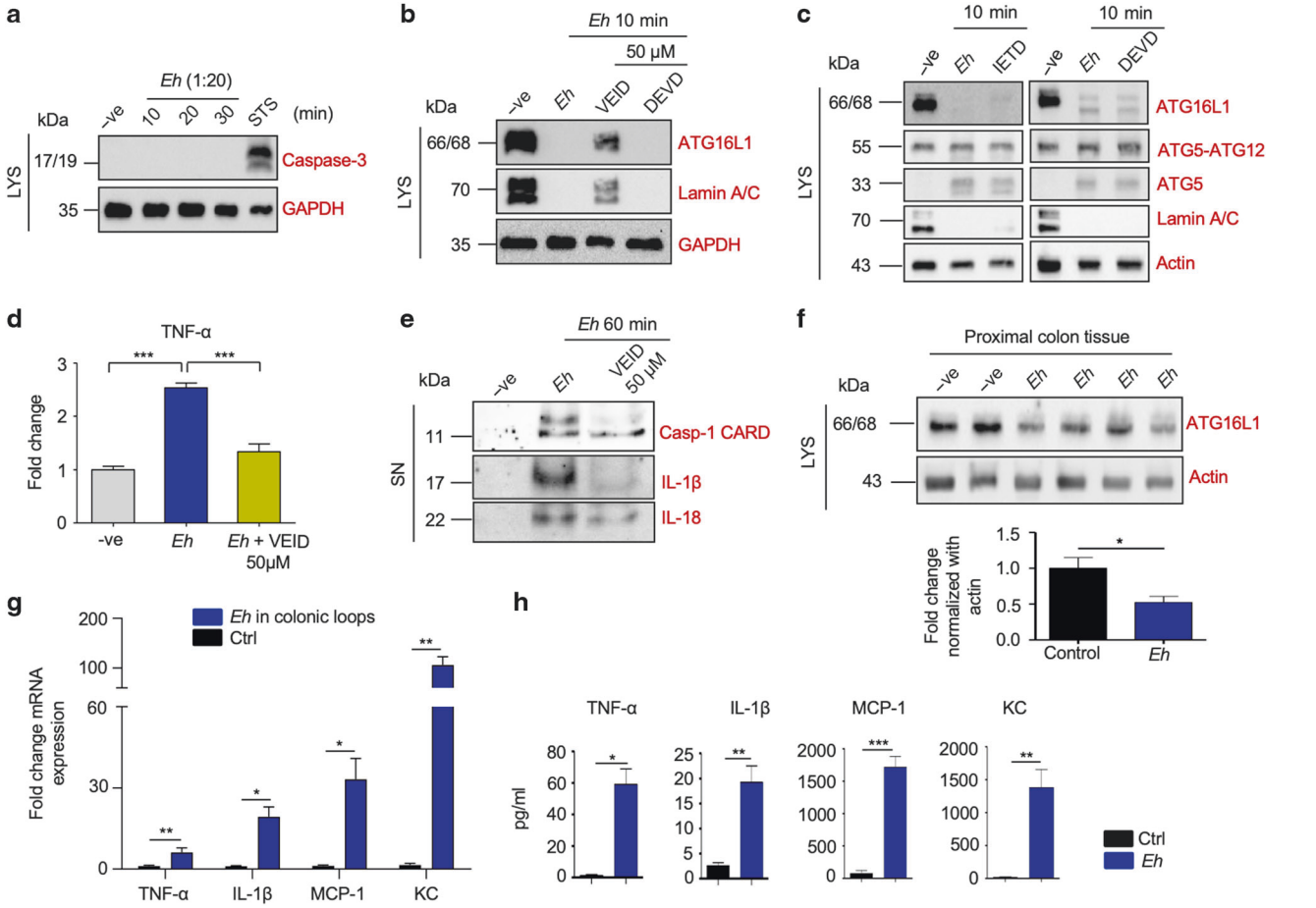

Fig. 4 Caspase-3/-8 independent ATG16L1 protein degradation and induction of pro-inflammatory responses. a THP-1 macrophages were stimulated with *Eh* for different time points to detect caspase-3 activation. **b** THP-1 macrophages were pre-treated with caspase-6 and caspase-3 inhibitor Z-VEID-fmk and Z-DEVD-fmk, respectively for 1 h with 50 μM concentration prior to stimulation with *Eh* for 10 min. ATG16L1 protein restoration was assessed by western blot along with lamin A/C restoration. **c** Bone marrow derived macrophages (BMDMs) were pre-treated with caspase-8 and caspase-3 inhibitor Z-IETD-fmk and Z-DEVD-fmk, respectively, for 1 h 50 μM concentration prior to stimulation with *Eh* for 10 min. ATG16L1 protein degradation was assessed by western blot along with ATG5 dissociation from ATG5-ATG12 conjugate and lamin A/C degradation. THP-1 macrophages were stimulated with *Eh* for 60 min in absence and presence of Z-VEID-fmk (50 μM) to detect **d**, TNF-α mRNA expression **e**, caspase-1 activation and IL-1β/IL-18 secretion. **f** Mouse proximal colon tissue from *Eh* (1 × 106) inoculated with 3 h closed colonic loops were quantified for ATG16L1 degradation by band densitometric measurement. **g** Pro-inflammatory cytokines and chemokines mRNA expression in corresponding colonic loop tissues after *Eh* inoculation. **h** Pro-inflammatory cytokines and chemokines secretion from BMDMs after *Eh* stimulation for 3 h. Cells without treatment is symbolized as (−ve). *Eh*-macrophage 1:20 ratio used for (**a**–**e**). Data are representative of at least three independent experiments ($n = 3$) and for statistical significance, *t*-test and one-way ANOVA followed by *post hoc* Bonferroni test was done. $^{*}P < 0.05$, $^{**}P < 0.01$, $^{***}P < 0.001$. Bars represent mean ± SEM.

increasing trend but was not significant (Supplementary Fig. S5b). To determine if *Eh* stimulated a more aggressive pro-inflammatory response in the ATG16L1 T316A variant as compared to WT, cytokines/chemokines were measured from BMDM in response to *Eh* stimulation that shown significantly enhanced levels of TNF-α, KC, and MCP-1 (Fig. 5e). IL-1β and IL-6 secretion was higher in both WT and ATG16L1 T316A variant BMDM (Supplementary Fig. S5d). These results show that both WT and ATG16L1 T316A variant are cleaved by caspase-6 and the presence of an SNP in the ATG16L1 (T300A in human, T316A in mice) gene, conferred increase susceptibility to *Eh*-induced degradation with enhanced pro-inflammatory cytokine release.

ATG16L1 protein is a proteolytic substrate for active CASP-6

Multiple sequence alignment analysis of human ATG16L1 protein discovered putative caspase recognition sites and various caspases could have overlapping sequence motifs in their substrate.[16,32] To determine whether ATG16L1 is a substrate for caspase-6, or if caspase-6 cleaves ATG16L1 protein directly, we quantified in vitro caspase cleavage with recombinant proteins. HA-tagged ATG16L1 protein was overexpressed in HEK293T cells and extracted by immunoprecipitation with anti-HA antibody. Immunoprecipitated ATG16L1 protein was incubated with active rCASP-6 and immunoblotted with both HA and ATG16L1 antibody showed degradation of ATG16L1 (Fig. 6a). As predicted, the addition of CASP-6 specific inhibitor (Z-VEID-fmk) completely rescued ATG16L1 degradation (Fig. 6a). We next sought to explore the degradation of constitutive ATG16L1 protein isolated from THP-1 macrophages. ATG16L1 protein was immunoprecipitated using ATG16L1 antibody and incubated with active rCASP-6 in the absence or presence of Z-VEID-fmk. Similar to transfected HEK293T cells, immunoprecipitated ATG16L1 from THP-1 macrophages showed degradation with rCASP-6 that was inhibited with Z-VEID-fmk (Fig. 6b). To confirm specificity for *Eh*-induced CASP-6 mediated ATG16L1 degradation, we transfected ATG16L1 in HEK293T cells followed by *Eh* stimulation in the absence or presence of different caspase inhibitors such as Z-VEID-fmk, Z-ZVAD-fmk, Z-DEVD-fmk, Z-IETD-fmk specific for caspase-6, pan-

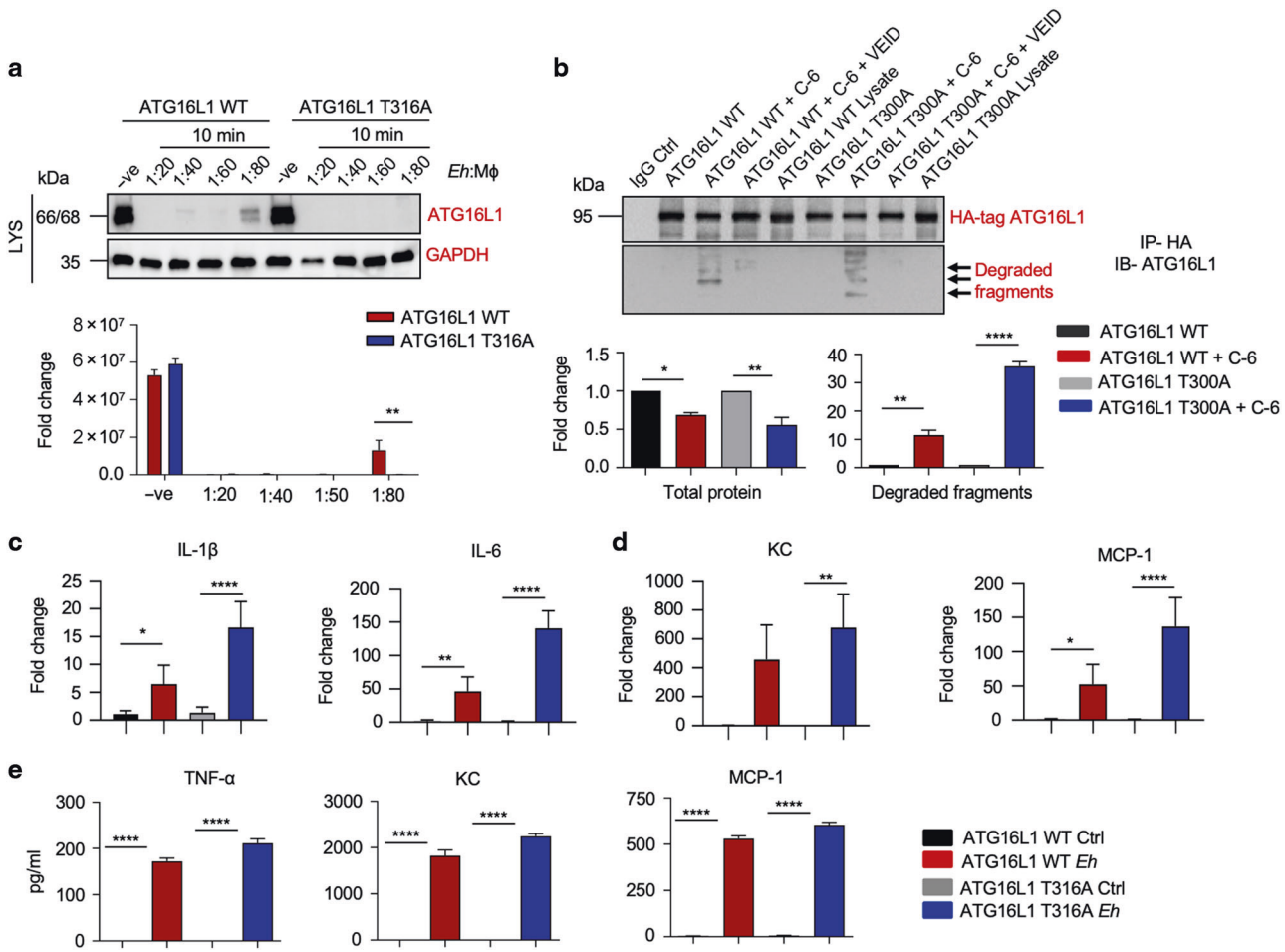

Fig. 5 Enhanced susceptibility of ATG16L1 T316A variant in response to *Eh*. Previously shown Crohn's disease associated ATG16L1 T300A variant (in mice corresponding SNP is at 316 position) is highly susceptible to *Eh* interaction. **a** BMDM cells from WT and ATG16L1 T316A variant were stimulated with different *Eh* to macrophage ratio for 10 min. **b** HEK293T cells were overexpressed with HA-tagged WT and ATG16L1 T300A variant and immunoprecipitated with anti-HA antibody. Immunoprecipitants were incubated 16 h at 37 °C with active recombinant caspase-6 in absence or presence of inhibitor Z-VEID-fmk (50 μM) and ATG16L1 cleavage was assessed by western blot with anti-ATG16L1 antibody and quantified by densitometric analysis. Direct cell lysate of WT (lane 5) and T300A variant (lane 9) were used as a control. mRNA expression of different pro-inflammatory cytokines and chemokines from *Eh* inoculated closed colonic loop tissues of WT and ATG16L1 T316A variant mice **c**, IL-1β and IL-6, **d**. KC and MCP-1. **e** Multiplex cytokine array by Luminex showed significantly increased TNF-α, KC and MCP-1 secretion in T316A BMDM cells stimulated with *Eh* for 3 h at 1:20 ration. Cells without treatment is symbolized as (−ve). Data are representative of at least three independent experiments ($n = 3$) and for statistical significance one-way ANOVA followed by *post hoc* Bonferroni test was done. *$P < 0.05$, **$P < 0.01$, ***$P < 0.001$, ****$P < 0.0001$. Bars represent mean ± SEM.

caspase, caspase-3, caspase-8, respectively. Only the caspase-6 specific inhibitor, Z-VEID-fmk along with Z-ZVAD-fmk restored ATG16L1 protein degradation in response to *Eh* (Fig. 6c). To exclude the impact of other caspases (particularly caspase-3/-8) on ATG16L1 degradation, we used the caspase-3 defective MCF-7 cell line and stimulated with *Eh* in the absence or presence of Z-VEID-fmk, Z-ZVAD-fmk and Z-IETD-fmk. As expected, in addition to Z-ZVAD-fmk, only Z-VEID-fmk, the caspase-6 inhibitor noticeably restored ATG16L1 degradation (Fig. 6d), which substantiates our earlier observation that ATG16L1 is a proteolytic substrate for caspase-6.

To identify the cleavage sites for caspase-6 on ATG16L1, we performed in vitro cleavage assays by incubating both GST-tagged human recombinant ATG16L1 (rATG16L1) and recombinant active caspase-6 (rCASP-6) together. By western blot analysis, both full length (84 kDa) and degraded fragments were detected with anti-ATG16L1 and anti-GST antibody (Fig. 6e). Recombinant ATG16L1 was N-terminally tagged with GST (Supplementary Fig. S6a) and the proteins detected with anti-GST antibody showed N-terminal degraded fragments of rATG16L1. With anti-ATG16L1 and anti-GST antibody, we observed comparable molecular weight degraded fragments (70, 40, and 36 kDa) (Fig. 6e). Protein sequencing by Edman degradation of the cleaved peptide fragments only identified amino acid calls for the major 70 kDa fragment (Fig. 6e). By multiple sequence alignment analysis, the acquired amino acid were aligned with the ATG16L1 sequence at glycine-489 aa position and within these sequences there was an aspartic acid (D) residue present at 495 aa position (Fig. 6f). Caspase-6 substrate specificity cleaves after an aspartic acid (D) amino acid residue[29] and by ExPASy, we computed the molecular weight of the peptide fragment as ~70 kDa, which corresponds to the degraded protein band (Fig. 6e). Based on this, a diagrammatic presentation of the degraded fragment which contain N-terminal GST sequence (blue, M1-K218) and ATG16L1 sequence (black, M85-D495) is shown (Fig. 6f).

To predict the cleavage sites of the 36 and 40 kDa N-terminal fragments, a cleavage specificity preference 'logo' for P4-P4' position (Supplementary Fig. S6b) was generated from 'MEROPS-the peptidase database' based on the specificity matrix table. This cleavage site 'logo' is a diagrammatic representation of specificity

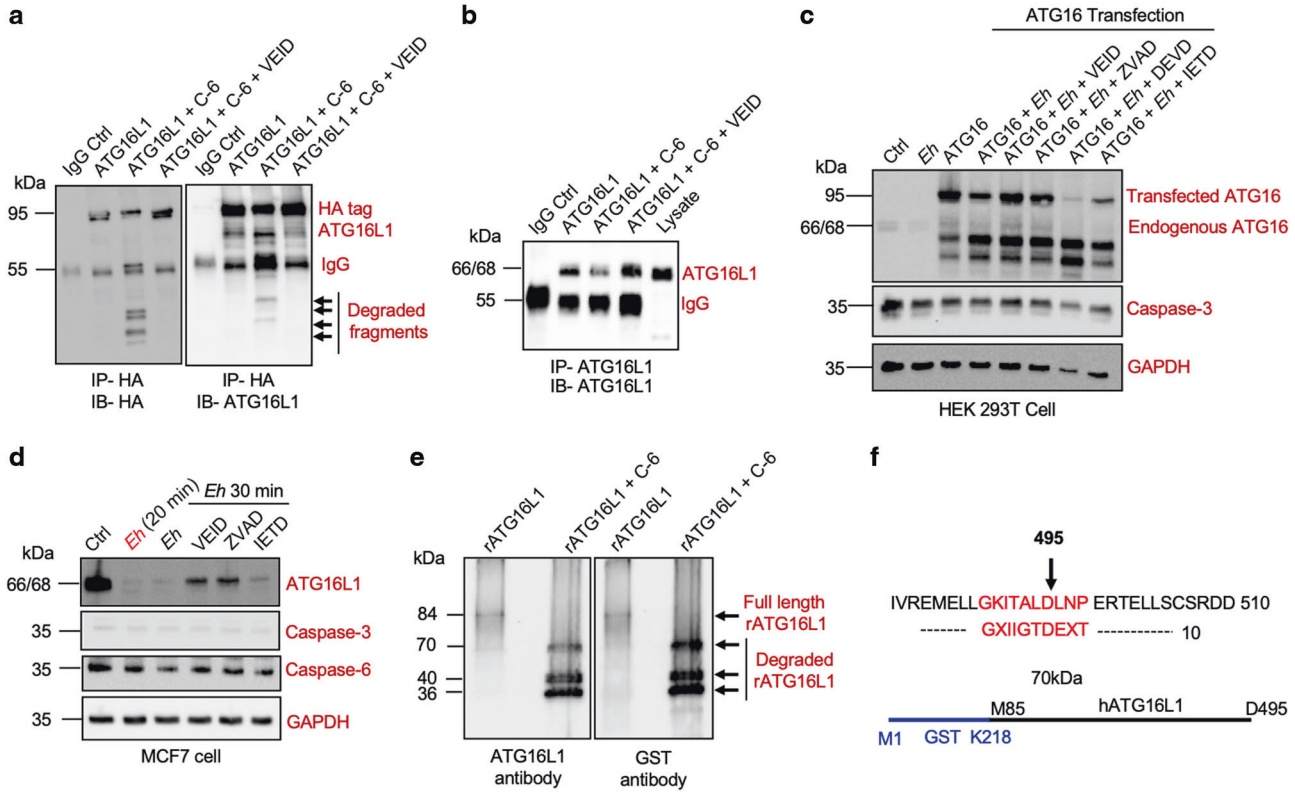

Fig. 6 In vitro cleavage of ATG16L1 by active recombinant caspase-6. a HA-tagged ATG16L1 were overexpressed in HEK 293T cells and immunoprecipitated with anti-HA antibody. Immunoprecipitants were incubated 16 h at 37 °C with active recombinant caspase-6 in absence or presence of inhibitor Z-VEID-fmk (50 μM) and ATG16L1 cleavage was assessed by western blot with anti-HA and anti-ATG16L1 antibody. **b** THP-1 macrophages were immunoprecipitated with anti-ATG16L1 antibody and immunoprecipitants were incubated 16 h at 37 °C with active recombinant caspase-6 in absence or presence of inhibitor Z-VEID-fmk (50 μM) and ATG16L1 cleavage was assessed by western blot with anti-ATG16L1 antibody. Direct cell lysate was used as a control (lane 5). **c** HA-tagged ATG16L1 overexpressed HEK 293T cells were incubated with *Eh* for 10 min in absence or presence of capspase-6 (Z-VEID-fmk), pan-caspase (Z-ZVAD-fmk), caspase-3 (Z-DEVD-fmk), caspase-8 (Z-IETD-fmk) inhibitors (50 μM) and ATG16L1 cleavage was assessed by western blot with anti-ATG16L1 antibody. **d** MCF-7 cells (caspase-3 defective cell line) were incubated with *Eh* for 20 min and with *Eh* for 30 min in absence or presence of capspase-6 (Z-VEID-fmk), pan-caspase (Z-ZVAD-fmk), caspase-8 (Z-IETD-fmk) inhibitor (50 μM) and ATG16L1 cleavage was assessed by western blot with anti-ATG16L1 antibody. Cells without treatment is symbolized as (Ctrl). *Eh*-macrophage 1:20 ratio used for (**c**, **d**). **e** N-terminal GST-tagged recombinant ATG16L1 incubated with recombinant active caspase-6 for 16 h at 37 °C and ATG16L1 degraded fragments were assessed by western blot with anti-ATG16L1 (M150-3, MBL international) and anti-GST antibody. Data are representative of at least three independent experiments ($n = 3$). **f** Sequence alignment of amino acid calls from Edman degradation analysis of 70 kDa band and schematic presentation of the fragment with a cutting site at aspartic acid 495 (D495) position. Blue line indicates GST protein (M1-K218) and black line for ATG16L1 (M85- D495).

preference of different amino acids present at the P4-P4′ positions during caspase-6 mediated cleavage. The preferable amino acid residues are presented in the usual one-letter code. Based on the specificity matrix 'logo' and the molecular weight of the bands detected by western blot we anticipated two putative cleavage sites for caspase-6 in ATG16L1 at aspartic acid (D) positions −167 (DEYD) and −212 (NEKD) (Supplementary Fig. S6c). Using ExPASy to compute the molecular weight, the predicted peptide fragments were 36 and 40 kDa, respectively (Supplementary Fig. S6c), which corresponds to the observed protein fragment bands in the western blot (Fig. 5e). Importantly, these three cleavage sites were exclusively distinct from the well-known caspase-3 specific cleavage site on ATG16L1 variant T300A at aspartic acid −299 (DNVD) position.[16]

Quantitative proteomics analysis of basal versus *Eh*-stimulated macrophage

To assess the global proteome changes in macrophages upon interaction with *Eh*, we performed a quantitative shotgun proteomics analysis of BMDMs. After 10 min *Eh* stimulation, protein lysates were digested with trypsin and naive macrophages were isotopically labeled with light formaldehyde (+28 Da) and macrophages + *Eh* with heavy formaldehyde (+34 Da; Fig. 7a). Data were analyzed using MaxQuant[33] at a 1% false discovery rate (FDR), and data integration for pathway and gene ontology (GO) enrichment was performed with Metascape,[34] and STRING-db.[35] For the interpretation, we describe changes in abundance of proteins as log2 (Mϕ + *Eh*: Mϕ), which means log2 values >0 represent proteins that were upregulated by Mϕ + *Eh*, <0 represent downregulation. In the proteomics analysis (Supplementary Table S1), we identified 81 unique proteins that were upregulated in response to *Eh*-macrophage interaction and 174 unique downregulated proteins. By using the online meta-analysis tool (metascape.org), we did a pathway enrichment and protein networking analysis within naive and *Eh* interacted macrophages and identified distinct pathways (Fig. 7b). As predicted, one of the downregulated pathways was autophagy and vesicle-mediated transport (highlight in blue, Fig. 7b), in accordance with our earlier observation of ATG16L1 protein complex alteration. Among the gene list of downregulated autophagy and vesicle-mediated transport pathway, 15 and 18 genes, respectively, corresponded to unique 174 downregulated proteins (Table 1). To understand the functional interactions between the downregulated/upregulated genes (15 genes and 18 genes), we used STRING-db v11 (https://string-db.org) and observed that majority of the downregulated proteins were clustered with membrane trafficking (blue

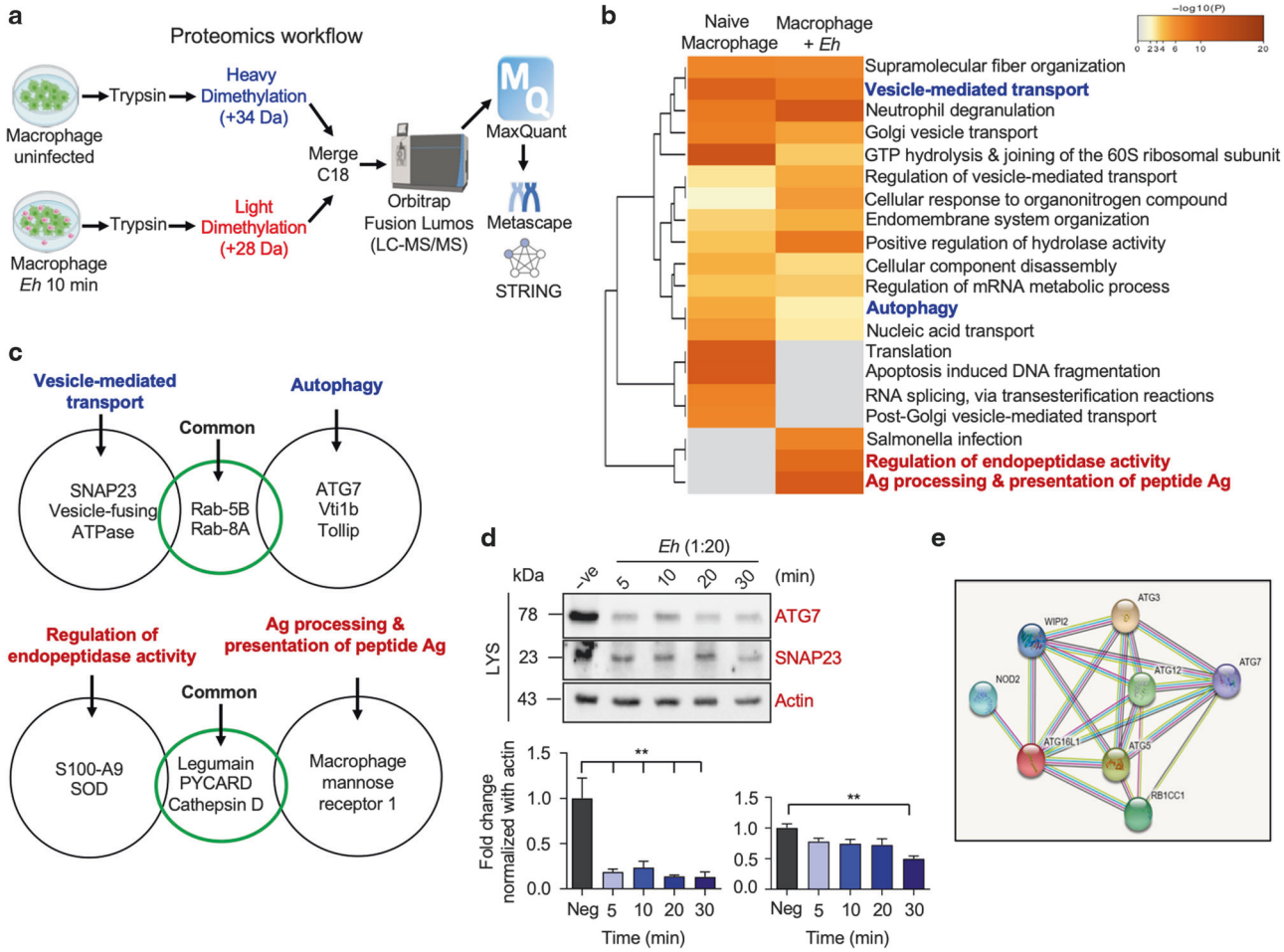

Fig. 7 Shotgun proteomics analysis of naive macrophage versus *Eh*-stimulated macrophage. a Shotgun proteomics protocol workflow. **b** Metascape analysis of different pathways between naive and *Eh*-stimulated macrophages. Blue marked are downregulated and red marked are upregulated pathways upon *Eh* interaction with macrophages. **c** Interesting protein hits identified within downregulated autophagy and vesicle-mediated transport pathways and with upregulated regulation of endopeptidase activity and antigen processing and presentation of peptide Ag pathways. **d** Bone marrow derived macrophages were stimulated with *Eh* for different time points and western blot done to detect ATG7 and SNAP23 levels in response to *Eh* and quantified by densitometric analysis. Cells without treatment is symbolized as (−ve). *Eh*-macrophage 1:20 ratio used. Data are representative of at least three independent experiments ($n = 3$) **e** STRING analysis of ATG16L1 protein-protein interaction with other known ATG proteins. $^{**}P < 0.01$.

nodes) and immune system (red nodes) reactome pathways (Supplementary Fig. S7a, b). Some interesting protein hits that were downregulated in response to *Eh* were ATG7, Ras-related proteins Rab8a, Rab5b, Snap23, vesicle-fusing ATPase, toll-interacting protein (Tollip), paxillin and vesicle transport through interaction with t-SNAREs homolog 1B (Fig. 7c, Table 2). Genetic deletion or knock down of ATG7 is linked with loss of autophagy,[36] thus we observed downregulation of autophagy process in response to *Eh* interaction. Different SNARE proteins also participate in autophagosome formation, autophagosome maturation, and autophagosome-lysosome fusion.[37] A recent study showed that SNAP23 interact with ATG16L1 and direct the ATG16L1-ATG12-ATG5 complex to the site of phagophore assembly and extension, thus depletion of SNAP23 impaired the autophagy process.[38] We validated negative regulation of ATG7 and SNAP23 in response to *Eh* by western blot in BMDM (Fig. 7d) and densitometric analysis showed significantly less ATG7 and SNAP23 compared to the negative control (Fig. 7d). THP-1 cells showed similar negative regulation of ATG7 protein in response to *Eh* (Supplementary Fig. S7c). By protein-protein network (STRING-db) analysis, ATG7 strongly interacts with ATG16L1, along with ATG5 and ATG12 (Fig. 7e), which convincingly support our observation.

From the meta-analysis of pathway enrichment, we also found regulation of endopeptidase activity and antigen processing and presentation of peptide antigen pathways were upregulated in response to *Eh* as compared to naive macrophages (marked in red Fig. 7b) and 24 and 5 genes, respectively, were matched to the unique 81 upregulated proteins (Table 1). Functional interaction analysis within the upregulated genes (24 genes and 5 genes) identified a dominant cluster of 16 proteins associated with immune system reactome pathway (red nodes) which supports our anticipation of elevated inflammatory responses (Supplementary Fig. S7b). Some upregulated protein hits in response to *Eh* were legumain, protein S100-A9, apoptosis-associated speck-like protein containing a CARD (ASC), macrophage mannose receptor 1, superoxide dismutase (SOD), and cathepsin D (aspartate endopeptidase) (Fig. 7c, Table 2). Among these proteins legumain was classified as a member of CPs with ~15% sequence homology to caspases and it has a strict specificity at the P1 position like caspases, though with a different preference for the P1-residue, Asn instead of Asp[39] Apart from its protease activity, legumain play important roles in immune signaling by proteolytically activating TLR receptors.[40,41] Extracellular S100-A9 act as an alarmin that binds pattern recognition receptors (PRRs) to activate the innate immune system and inflammatory responses.[42] ASC is

Table 1. Some of the attractive protein hits identified with downregulated and upregulated pathways upon *Eh* interaction with macrophages and their involvement in different biological processes.

Pathway	Proteins name	Gene name	Log2 (Mϕ + *Eh*:Mϕ)
Autophagy	Ras-related protein Rab-8A	Rab8a	−2.487297773
	Vesicle transport through interaction with t-SNAREs homolog 1B	Vti1b	−2.276415228
	Leucine-rich PPR motif-containing protein, mitochondrial	Lrpprc	−1.920352236
	Ubiquitin-like modifier-activating enzyme ATG7	Atg7	−1.879435719
	Eukaryotic translation initiation factor 4 gamma 2	Eif4g2	−1.869596238
	Phosphatidylinositol 5-phosphate 4-kinase type-2 alpha	Pip4k2a	−1.696330289
	DDRGK domain-containing protein 1	Ddrgk1	−1.375571523
	Casein kinase II subunit alpha	Csnk2a1	−1.357825241
	Vacuolar protein-sorting-associated protein 13C	Vps13c	−1.329413427
	Nicotinamide phosphoribosyltransferase	Nampt	−1.264269882
	Nuclease-sensitive element-binding protein 1	Ybx1	−1.250989274
	Protein LYRIC	Mtdh	−1.240315772
	Vacuolar protein-sorting-associated protein 25	Vps25	−1.215713799
	Toll-interacting protein	Tollip	−1.134730445
	Mitochondrial import receptor subunit TOM40 homolog	Tomm40	−1.121109901
Vesicle-mediated transport	Apolipoprotein E	Apoe	−3.51414455
	COP9 signalosome complex subunit 5	Cops5	−3.304576253
	Guanine nucleotide exchange factor for Rab-3A	Rab3il1	−2.78061151
	Serine/threonine-protein phosphatase 6 regulatory subunit 1	Ppp6r1	−2.364162044
	Arf-GAP domain and FG repeat-containing protein 1	Agfg1	−1.862706338
	Sorting nexin-9	Snx9	−1.746180117
	Vesicle-fusing ATPase	Nsf	−1.562175701
	N-acetylglucosamine-6-sulfatase	Gns	−1.489078578
	Ras-related protein Rab-5B	Rab5b	−1.44575498
	ADP-ribosylation factor GTPase-activating protein 2	Arfgap2	−1.392212831
	Spectrin beta chain, non-erythrocytic 1	Sptbn1	−1.382889625
	Synaptosomal-associated protein;Synaptosomal-associated protein 23	Snap23	−1.316635909
	Endophilin-A2	Sh3gl1	−1.303009113
	AP-3 complex subunit sigma-1	Ap3s1	−1.267496341
	Ras-related protein Rab-14	Rab14	−1.212935361
	Tubulin alpha-1B chain	Tuba1b	−1.203070057
	Actin, cytoplasmic 1;Actin, cytoplasmic 1, N-terminally processed	Actb	−1.18590081
	Protein ERGIC-53	Lman1	−1.066276302
Regulation of endopeptidase activity	Biquitin carboxyl-terminal hydrolase;Ubiquitin carboxyl-terminal hydrolase 14	Usp14	0.977023422
	Cathepsin D	Ctsd	0.98112199
	Importin-5	Ipo5	1.03083043
	Mitochondrial fission 1 protein	Fis1	1.089226942
	Proteasome activator complex subunit 2	Psme2	1.132905812
	Tyrosine-protein phosphatase non-receptor type 1	Ptpn1	1.157819839
	40S ribosomal protein S6	Rps6	1.172423508
	Superoxide dismutase [Cu-Zn]	Sod1	1.173319354
	Peroxiredoxin-6	Prdx6	1.219586745
	Apoptosis-associated speck-like protein containing a CARD	Pycard	1.291603558
	Trifunctional purine biosynthetic protein adenosine-3;Phosphoribosylamine--glycine ligase;Phosphoribosylformylglycinamidine cyclo-ligase; Phosphoribosylglycinamide formyltransferase	Gart	1.325271271
	Ubiquitin-conjugating enzyme E2 K	Ube2k	1.380064459
	Lysosome-associated membrane glycoprotein 1	Lamp1	1.403758537
	Cystatin-B	Cstb	1.624709202
	Phosphatidylethanolamine-binding protein 1;Hippocampal cholinergic neurostimulating peptide	Pebp1	1.633663697
	E3 SUMO-protein ligase RanBP2	Ranbp2	1.757492686

Table 1. continued

Pathway	Proteins name	Gene name	Log2 (Mϕ + *Eh*:Mϕ)
	GTP-binding protein SAR1b	Sar1b	1.887954116
	Glutathione peroxidase 1;Glutathione peroxidase	Gpx1	2.001946325
	Legumain	Lgmn	2.113433803
	Protein S100-A9	S100a9	2.188211001
	Allograft inflammatory factor 1	Aif1	2.227956663
	GTPase-activating protein and VPS9 domain-containing protein 1	Gapvd1	2.287058517
	AP-2 complex subunit mu	Ap2m1	2.339736008
	Acidic leucine-rich nuclear phosphoprotein 32 family member B	Anp32b	3.002324472
Antigen processing and presentation of peptide antigen	26S proteasome non-ATPase regulatory subunit 13	Psmd13	0.96842258
	Ras-related protein Rab-7a	Rab7a	1.039419183
	Cytoplasmic dynein 1 light intermediate chain 1	Dync1li1	1.117828004
	Proteasome subunit beta type-7	Psmb7	1.243730004
	Macrophage mannose receptor 1	Mrc1	2.327256216

an adaptor protein of inflammasome activation that triggers IL-1β/IL-18 secretion that supports our previous observation of *Eh*-induced inflammasome activation and robust pro-inflammatory responses.[2,9] Macrophage mannose receptor 1 act as a PRR of the innate immune system, able to bind pathogens and stimulate downstream immune responses.[43] Upregulation of this receptor in response to *Eh* supports our earlier observation of inflammatory responses. *Eh*-macrophage interaction induces oxidative stress and to control this stress response the induction of SOD is required.[44,45] Thus, through the quantitative proteomics analysis we have identified downregulation of autophagy and vesicle-mediated transport processes in addition with the anticipated upregulation of cysteine/aspartate proteases and inflammatory responses during *Eh*-macrophage interaction.

DISCUSSION

The molecular events at the *Eh*-macrophage intercellular junction that initiates high output pro-inflammatory cytokine production in disease pathogenesis is not well understood. In this study we unraveled that the autophagy ATG16L1 protein complex was proteolytically cleaved by caspase-6 at the *Eh*-macrophage intercellular junction resulting in global negative regulation of host autophagy processes that exacerbated pro-inflammatory cytokine responses. In this interaction, ATG16L1 was discovered as a novel proteolytic substrate for active caspase-6 and that Crohn's disease associated ATG16L1 variant (T300A in human, T316A in mice) was highly susceptible to *Eh*-mediated degradation that enhanced pro-inflammatory cytokine responses in an animal model of disease. These findings have unmasked a novel immunoregulatory role for the essential autophagy protein ATG16L1 as a master regulator for pro-inflammatory cytokine responses in *Eh* disease pathogenesis. Thus, autophagy maybe an overlooked process that extracellular parasites use for outside-in signaling to evoke pro-inflammatory cytokines.

Autophagy is an intracellular degradation process with a housekeeping role of removing or clearing misfolded or aggregated proteins, damaged organelles such as mitochondria, endoplasmic reticulum, and intracellular pathogens.[46] Functioning autophagy is essential for regulating inflammatory responses. Deficiency in autophagy leads to the accumulation of aged and dysfunctional mitochondria that produce excess reactive oxygen species (ROS) and excessive activation of NLRP3 inflammasome upon stimulation.[19,47] In addition, deficiency in autophagy exacerbate colitis, sepsis, pneumonia, and urinary tract infection with enhanced inflammasome mediated IL-1β and IL-18 production.[19,48,49] ATG16L1 is a vital component of the core autophagy process and play key roles in regulating pro-inflammatory responses. Hypomorphic ATG16L1 mice showed abnormalities in Paneth cells with irregular granule morphology and increased inflammatory gene expression.[50] ATG16L1 deficient macrophages showed enhanced caspase-1 activation and IL-1β/IL-18 secretion in response to endotoxin LPS and loss the capacity of cells to form autophagosome.[15] Patients with ATG16L1 T300A variant produce elevated amount of IL-1β upon muramyl dipeptide stimulation compared to WT ATG16L1.[51] Conditional knockout of ATG16L1 in epithelial cells abrogate autophagy process and displayed susceptibility to *Salmonella enterica* serovar Typhimurium infection.[52] The presence of intact ATG16L1 is critical to maintain the autophagy process, to control inflammatory responses and to tackle infection with gut microbes. The role of ATG16L1 deficiency or mutation were mostly interrogated in response to intracellular pathogens, here we observed that the extracellular parasite *Eh* uses outside-in signaling to trigger rapid time- and dose-dependent degradation of ATG16L1 protein and dissociation of ATG5 from ATG12-ATG5 conjugate and subsequent downregulation of autophagy process. ATG16L1 is known as ATG5-binding protein and during autophagy, intact ATG16L1 is required for the formation of high molecular weight (~800 kDa) protein complex with ATG12-ATG5 conjugate.[23,24] We hypothesize that rapid degradation of ATG16L1 allowed ATG5 to dissociate from the intact complex that escalated pro-inflammatory cytokine responses. Restoration of ATG16L1 downregulated TNF-α expression and suppressed IL-1β/IL-18 production as well as caspase-1 activation in response to *Eh*. From quantitative proteomics analysis we observed downregulation of key proteins directly involved with autophagy process. One of the hits, ATG7 which has direct protein-protein interaction with ATG16L1 protein complex, act as an ATP dependent manner to activate ATG12 through the formation of a high-energy thioester bond between the C-terminal glycine of ATG12 and the active cysteine of ATG7. Subsequently, activated ATG12 is transferred to the ATG5 protein to form the final ATG12-ATG5 conjugation which followed by association with ATG16L1 protein.[14] Deficiency of ATG7 results an explicit loss of autophagy.[36] Intestinal epithelial cell specific deletion of ATG7 showed affects on mucosal microenvironment and linked to alteration of the microbiota composition.[53] Thus, *Eh*-mediated downregulation of ATG7 might have broader impact as studies have showed alteration in microbiota composition.[54–56] The Rab proteins belongs to the Ras-like GTPases and vesicle fusion

Table 2. Selected proteins that were differentially regulated in response to *Eh*-macrophage interaction.

	Protein names	Biological process (GO)
Downregulated	ATG7	Autophagy; Regulation of vesicle-mediated transport; Regulation of response to stimulus; Regulation of signaling
	Rab-5B	Vesicle organization; Regulation of vesicle-mediated transport
	Rab-8A	Autophagy; Vesicle fusion and organization; Regulation of vesicle-mediated transport; Regulation of signaling
	Vti1b	Vesicle fusion and organization
	SNAP23	Vesicle fusion and organization; Regulation of vesicle-mediated transport
Upregulated	Toll-interacting protein	Autophagy
	Paxillin	Regulation of response to stimulus; Regulation of signaling
	Legumain	Activation of cysteine-type endopeptidase activity; Positive regulation of response to stimulus
	S100-A9	Regulation of cysteine-type endopeptidase activity; Immune system process
	PYCARD	Activation of cysteine-type endopeptidase activity; Positive regulation of response to stimulus; Signal transduction
	Macrophage mannose receptor 1	Innate immune response; Signal transduction
	SOD	Response to oxidative stress; Positive regulation of response to stimulus; Homeostatic process
	LAMP 1	Positive regulation of response to stimulus; Signal transduction; positive regulation of exocytosis
	Cathepsin D	Autophagosome assembly

proteins known SNAREs have been shown to be involved in various stages of autophagy such as autophagosome formation and maturation. Rab proteins are well-known regulators of membrane trafficking and fusion processes that play defined roles in autophagy such as RAB5 play role in conjugation of ATG12 with ATG5 via its effector and regulate autophagosome formation.[57,58] Inhibition of Rab5 reduces the ATG12-ATG5 conjugation and knock down of Rab5 shown significantly decreased LC3-II formation in response to hepatitis C virus NS4B protein.[59,60] Similarly, RAB8 play a role in autophagosome maturation during antimicrobial autophagy.[61] Vesicle transport through interaction with t-SNAREs homolog 1B (Vti1b) is involved in the autophagosome-lysosome fusion as depletion of this protein have been shown inhibit autophagic degradation.[62] Tollip function as an adaptor molecule in the Toll-like receptor (TLR) signaling pathway and reduced Tollip level is associated with disruption of autophagosome-lysosome fusion in macrophages.[63] We have previously shown cytoskeleton associated protein paxillin is degraded at the intercellular junction between *Eh*-macrophage and act an immune sensor to trigger downstream inflammatory responses via IL-1β secretion.[11] Along with the autophagy process, we observed negative regulation of vesicle-mediated transport pathways which corroborates our findings on dysregulated autophagy in response to *Eh*. Simultaneously, we observed upregulation of different cysteine-type endopeptidase activity such as Legumain, aspartate endopeptidase Cathepsin D and inflammatory molecules S100-A9, PYCARD, which all are directly involved with the biological process to regulate immune responses (Table 1).

Degradation of ATG16L1 protein was observed only when macrophages interacted with live *Eh* via Gal-lectin adhesion. These results were similar to previously observed NLRP3 inflammasome activation and cytoskeletal-associated protein degradation.[2,11] Stimulation with purified native Gal-lectin was not sufficient to induce ATG16L1 protein degradation that suggest other *Eh* molecules at the intercellular junction are critically involved in downstream signaling. Consistent with this, we found that *Eh* CPs, *Eh*CP-A1 and *Eh*CP-A4 individually or together, delivered the critical signal that initiated ATG16L1 protein degradation. These results are strikingly similar to our previous observations where *Eh*-induced rapid cytoskeletal-associated protein degradation at the site of contact.[11] *Eh*CP-A1 and *Eh*CP-A4 are localized into intracellular vesicles[26,64] and during *Eh*-macrophage interactions, the Gal-lectin form a bridge allowing the CPs to polarize at the contact site.[11] *Eh* virulent factors, Gal-lectin and different cysteine proteinases mediate the dynamic cross-talk of cytoskeletal protein degradation at the intercellular junction and activation of the NLRP3 inflammasome,[2,9] caspases,[10] and alarmin molecule secretion.[65] *Eh* outside-in signaling initiated by the surface Gal-lectin and *Eh*CP-A1/*Eh*CP-A4 polarization towards the interface of *Eh*-macrophage allows the parasite to downregulate host regulatory autophagy proteins. Most importantly, only live parasites mediated direct interaction with macrophages to deliver the downstream signaling outcomes.

Caspase-6 is categorized as an apoptotic effector caspase along with caspase-3 and caspase-7.[66] Caspase-6 play important roles in innate immunity beyond apoptosis. Caspase-6 reduces the expression of the immunosuppressant cytokine IL-10[67] and induces TNF-α release through cleavage of macrophage suppressor IRAK-M upon inflammatory stimulation.[68] Caspase-6 knockout mice are protected from septic shock mediated death and have reduced TNF-α level following LPS stimulation.[68,69] Caspase-6 also induces alterations in cytoskeletal-associated proteins and IL-1β secretion in response to *Eh*.[11] Importantly, our study revealed another critical proteolytical cleavage function for caspase-6 in response to *Eh*. The molecular mechanism for ATG16L1 protein degradation in response to *Eh* was mediated by caspase-6 activation as both siRNA silencing and inhibition of enzyme activity with Z-VEID-fmk restored protein degradation. These findings support the notion that *Eh*-induced caspase-6 activation is critical in disease pathogenesis as it triggers rapid proteolytic degradation of ATG16L1 to enhance pro-inflammatory cytokines and chemokines secretion. Intriguingly, activation of caspase-6 was independent of active caspase-3, and is consistent with other studies showing caspase-6 can undergo autoactivation in vitro and in vivo in the absence of caspase-3.[28,29] Similarly, upon *Eh* interaction with macrophage, both activation and function of caspase-6 was independent of caspase-8, which is another highly caspase-6 interacting protein, detected in the protein-protein network assessment. The mechanism of *Eh*-induced caspase-6 activation is not fully known, but based on our previous findings[11] and the results of the current study, we propose that upon live *Eh*-macrophage interaction at the intercellular junction, dynamic actin rearrangement occurs which may provide the functional

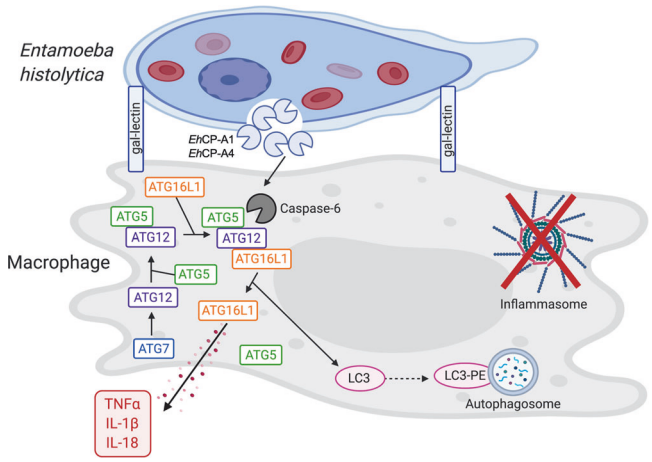

Fig. 8 Schematic representation of *Eh*-macrophage interactions at the intercellular junction with downstream effects (altered autophagy) and outcome (enhanced inflammatory responses). At the intercellular junction between *Eh*-macrophage, *Eh* contact with macrophage through cell surface adhesin Gal-lectin mediates high affinity binding. Simultaneously, *Eh*CP-A1 and *Eh*CP-A4, localized within intracellular vesicles, polarized to the *Eh*-macrophage contact site to activate caspase-6, which is independent of *Eh*CP-A5. Activated caspase-6 induce degradation of the autophagy ATG16L1 protein complex composed of ATG16L1 and ATG5-ATG12 conjugate. ATG12-ATG5 conjugate formation requires ATG7, which activate ATG12 to interact with ATG5. *Eh*-induced active caspase-6 trigger dissociation of ATG5 protein from the ATG12-ATG5 conjugate. *Eh*-macrophage interaction downregulate ATG7 which can also interfere with ATG16L1-ATG12-ATG5 complex formation. ATG16L1 protein complex is vital for the downstream LC3 conjugation with phosphatidylethanolamine (PE) for autophagosome formation. In disease pathogenesis, ATG16L1 is a proteolytic substrate for *Eh*-activated active caspase-6 and modulate the immune regulatory process autophagy-associated proteins to potentiate the host inflammatory responses by increased secretion of TNF-α, IL-1β and IL-18 in an inflammasome independent manner.

activation signal for different host proteinases. In support of this, inhibition of actin polymerization with cytochalasin D abrogated caspase-6 activation. Simultaneously, both *Eh*CP-A1 and *Eh*CP-A4 are polarized towards the *Eh*-macrophage contact point[11] and inhibition of these CPs strongly reduced caspase-6 activation. Thus, we assume cross-talk between *Eh*CPs and host cell cytoskeletal dynamics assimilate the signal for caspase-6 activation.

An SNP in the ATG16L1 gene (Thr300Ala in human, Thr316Ala in mice) renders strong association with susceptibility to Crohn's disease and increase sensitization to caspase-3 mediated degradation resulting in elevated levels of pro-inflammatory cytokines TNF-α, IL-1β, IL-6 in response to *Yersinia enterocolitica* infection.[16] ATG16L1 T300A variant carriers are associated with increased danger for hepatitis B infection.[70] Interestingly, we found that in response to *Eh*, BMDM cells with ATG16L1 T316A variant were significantly susceptible for degradation as compared to WT ATG16L1. Similarly, ATG16L1 T316A mice significantly augmented pro-inflammatory cytokines and chemokines expression in colonic loops infected with *Eh*. These findings are new to *Eh* pathogenesis, as previously polymorphisms in the leptin (satiety hormone) gene have been shown to be associated with increased susceptibility to amebiasis.[71,72] The in vivo colonic loop study with *Eh* inoculation in WT and ATG16L1 T316A variant mice delineate a new genetic susceptibility association with *Eh* infection and/or invasive disease.

The cleavage motifs recognized by different caspases are similar in their substrates and multiple sequence alignment analysis discovered the presence of putative caspase target sequences on ATG16L1.[16] Caspase-3 mediated ATG16L1 processing was reported in response to apoptotic induction.[16,32] In our study, in response to *Eh*, caspase-3 activation and apoptosis was not observed and over expression of caspase-6 and caspase-6 activity in HEK293T cells did not trigger cell death.[28] In addition to *Eh*-stimulated caspase-6 mediated ATG16L1 protein degradation, in vitro cleavage assays confirmed that ATG16L1 protein is a proteolytic substrate for active caspase-6. Furthermore, by utilizing recombinant ATG16L1 and caspase-6, we identified three main degraded fragments and based on Edman sequencing we identified one cleavage site position at amino acid aspartic acid 495 (70 kDa fragments). A shortcoming of the Edman sequencing revealed it was not able to interpret amino acids present on the other two fragments due to weak signals. To overcome this, we utilized peptidase database matrix table generated based on caspase-6 cleavage sequence specificity and preference and predicted putative cleavage sites on the ATG16L1 protein. Interestingly, these putative cleavage sites are completely different from caspase-3 specificity. Caspase-6 is associated with different neurological disorders by cleaving neuronal proteins that made it a critical molecular target to treat neurological disorders.[73,74] Similarly, at the intercellular junction between *Eh*-macrophage, active caspase-6 triggered rapid degradation of the autophagy protein ATG16L1 complex to induce alteration in host homeostatic regulatory process autophagy that potentiate uncontrolled pro-inflammatory responses (Fig. 8). This is a novel finding in *Eh*-host interaction and has uncovered several molecular targets for immunologic and/or therapeutic intervention in the control of *Eh*.

MATERIALS AND METHODS

E. histolytica culture and preparation

E. histolytica virulent strain, HM-1:IMSS were grown axenically in TYI-S-3 medium supplemented with 100 U/ml penicillin and 100 µg/ml streptomycin sulfate in sealed 15 ml borosilicate glass tubes at 37 °C as illustrated previously.[75] After 72 h of log-phase growth, *Eh* were harvested by placing on ice for 5 min and then centrifuged at 200 × *g* for 5 min at 4° C. After centrifugation, *Eh* were resuspended in serum-free RPMI to count and prepared a final cell suspension of 1 × 106 *Eh*/ml. *Eh*CP-A5 deficient amoeba were a generous gift from Dr. David Mirelman (Weizmann Institute of Science, Rehovot, Israel) and cultured similarly.

Cell culture and stimulation

To culture THP-1 human monocytic cell line (ATCC), complete RPMI medium (supplemented with 10% FBS, 10 mM HEPES, 50 µM β-mercaptoethanol, 100 U/ml penicillin, and 100 µg/ml streptomycin sulfate) was used in a humidified cell culture incubator with 5% CO_2. THP-1 cells at 8 × 105 /well were plated into 12-well tissue culture plates for overnight in complete medium supplemented with 50 ng/ml phorbol-12-myristate-13-acetate (PMA) to differentiate into macrophages. For *Eh* stimulation, complete RPMI medium from the plate were replaced with serum-free RPMI and incubated with *Eh* for indicated time and ratio at 37 °C. For inhibitor experiments, overnight PMA differentiated macrophages were pre-treated with inhibitors for indicated concentrations and time prior to *Eh* stimulation. For Gal-lectin adhesion inhibition experiment, *Eh* were pre-treated with 55 mM exogenous D-galactose for 5 min prior incubation with THP-1 macrophages. For *Eh* CP function inhibition experiment, *Eh* were pre-treated overnight with 100 µM of E-64, as previously described.[76] For *Eh*CP-A1 and *Eh*CP-A4 activity inhibition study, *Eh* were pre-incubated with 20 µM of WRR483 and 20 µM of WRR605, respectively or both together for 30 min before stimulation with THP-1 macrophages. After *Eh* stimulation, plates were washed with cold PBS and lysis buffer (1% Triton X-100, 20 mM Tris,

100 mM NaCl, 1 mM EDTA, 200 mM orthovanadate, sodium fluoride, 0.1% SDS, PMSF, leupeptin, aprotinin, and protease inhibitor cocktail) was added to lyse the cells. Protein concentrations were measured by the bicinchoninic acid protein assay kit with standards (Thermo Scientific, Catalog No. CAPI23225).

CASP1 and CASP4 CRISPR/Cas9 KO THP-1 cell was a gift from V. Hornung (Institute of Molecular Medicine, University Hospital, University of Bonn, Germany). To generate this cell, CMV-mCherry-CAS9 expression cassette encoded plasmid and a gRNA under the U6 promoter was used. The CRISPR target regions were: ATTGACTCCGTTATTCCGAA**AGG** (CASP1) and GCTCATCCGAA-TATGGAGGC**TGG** (CASP4). CRISPR KO cells were cultured in complete RPMI media as mentioned earlier.

To culture human colonic T84 epithelial cell (ATCC), DMEM F12 (1:1) supplemented with 10% FBS, 100 U/ml penicillin and 100 µg/ml streptomycin sulfate was used in a cell culture incubator with 5% CO_2. For experiments, 3×105 cells/well were plated in 12-well plates to grow as 80% cell confluence.

BMDM preparation and stimulation

BMDMs were prepared from the femurs and tibias of 8–10-weeks-old C57BL/6 mice or indicated knockout or mutant mice and cultured for 6 days in complete RPMI medium supplemented with 30% L-929 cell supernatant. After 6 days, 8×105 cells/well were plated in a 12-well plate for overnight with complete RPMI medium. On the day of *Eh* stimulation, complete medium was replaced with serum-free RPMI and incubated with *Eh* for indicated time and ratio.

Amebic secretory proteins, whole lysate, cytosolic and membrane components preparation

2×107 *Eh*/ml were incubated with Hank's balanced salt solution (HBSS) for 2 h at 37 °C to prepare the secreted proteins. For other experiments, equal amounts of fresh live *Eh* were freeze-thawed three times in Hank's balanced salts solution to prepare whole lysates. Similarly, centrifugation of freeze-thawed *Eh* lysates at 4 °C for 15 min at $14{,}000 \times g$ was used to generate cytosolic and membrane components. Supernatants were collected as cytosolic fractions and the resuspended pellets were used as membrane fractions.

Immunoprecipitation

For THP-1 macrophage cell immunoprecipitation, anti-ATG16L1 antibody (1:300, cell signaling),) was used to pull down proteins from cell lysate in the presence of 10% A/G beads (Santa Cruz) at 4 °C. Protein-bead complexes were washed 5–6 times with lysis buffer and samples were boiled at 95 °C for 5 min. Immunoblots were done by using two different anti- ATG16L1 antibody.

Caspase-6 siRNA

THP-1 monocytic cells were transfected with 50 nM caspase-6 siRNA or scramble siRNA as a control (Dharmacon) with nuclear factor technique according to the manufacturer's protocol. After siRNA transfection, cells were differentiated with PMA. Every 24 h media was replaced with new complete RPMI. After 48 h following siRNA transfection, cells were stimulated with *Eh* for 5 min to assess ATG16L1 protein degradation.

Western blots

Equal amounts of cell lysates were used to load on SDS-PAGE gel and transferred into nitrocellulose membrane. Membranes were blocked with 5% skim milk followed by overnight incubation with indicated primary antibodies at 4 °C. Next day, followed by 1 h HRP-conjugated secondary antibody incubation, membranes were visualized with either SuperSignal Chemiluminescence Reagents (Pierce Biotechnology) or ChemiLucent ECL detection (EMD Millipore). For the detection of loading control protein (GAPDH or Actin), membranes were incubated with stripping solution (25 mM Glycine, 1% SDS, pH 2.0) for 30 min. After washing, again blocked with 5% skim milk followed by primary antibody incubation. A complete list of antibodies is included in Supplementary Table S3.

Immunofluorescence

THP-1 cells were grown on cover slips and stimulated with *Eh* for 10 min. After stimulation, cells were washed gently with PBS and fixed with 3% paraformaldehyde for 10 min. Cell permeabilization done with 0.01% triton in PBS for 5 min followed by blocking with 2% donkey serum for 1 h. Cells were stained with rabbit anti-ATG16L1 antibody overnight at 4 °C. Next day cells were washed gently with PBS-Tween (0.1%) and incubated with DAPI and secondary antibody at room temperature for 1 h. The cover slips with cells were mounted onto microscope slides with FluoroSave™ reagent (Calbiochem) and imaged using Olympus IX81 FV1000 Fluoview Laser Scanning Confocal microscope with a ×60 objective. Image preparation and quantification of the cytoplasmic ATG16L1 mean intensity was achieved in ImageJ software.

HEK293T transfection and in vitro caspase-cleavage assay

HEK293T cells (2.5×10^5/well) were grown in six well plates and transfected with 1 µg expression plasmids for HA-tagged WT and T300A variant of ATG16L1 by jetPRIME Polyplus transfection reagent. After 24 h cell lysates were collected and immunoprecipitated with anti-HA antibody followed by protein A/G Sepharose beads conjugation. Coupled protein bound beads were re-suspended into caspase cleavage buffer (50 mM HEPES, pH 7.2, 50 mM NaCl, 0.1% CHAPS, 10 mM EDTA, 5% glycerol and 10 mM DTT). 2U active recombinant human caspase-6 was incubated with the isolated proteins for 16 h at 37 °C. For inhibitor experiment, 50 µM caspase-6 inhibitor Z-VEID-fmk was added for 10 min at room temperature prior to recombinant caspase-6 incubation. After 16 h, samples were examined by western blot with both anti-HA and anti-ATG16L1 antibodies.

Edman protein sequencing

Active recombinant caspase-6 and GST-tagged human recombinant ATG16L1 were incubated together for 16 h at 37 °C. After 16 h, samples were run on SDS-PAGE gel and transferred into PVDF membrane. Coomassie blue staining was used to visualize the degraded fragments. After drying, fragments bands were cut and send for Edman sequencing at Tufts University core facility.

Shotgun proteomics analysis

Naive macrophages and *Eh* interacted (10 min) macrophages were used for shotgun proteomics analysis. Protein samples were lysed with 1% SDS, 0.1 M EDTA in 200 nM HEPES (pH 8), protease inhibitor tablets (Roche). Proteins were denatured with the addition of a final concentration of 10 mM DTT. Samples were alkylated by incubation with a final concentration of 15 mM iodoacetamide in the dark for 25 min at room temperature. With HCl the pH adjusted to 6.5. Next, to label peptide α- and ε-amines, samples were incubated for 18 h at 37 °C with isotopically heavy [40 mM $^{13}CD_2O + 20$ mM $NaBH_3CN$ (sodium cyanoborohydride)] or light labels [40 mM light formaldehyde (CH_2O) + 20 mM $NaBH_3CN$], all final concentrations. Samples were subjected to C18 chromatography before being subjected to liquid chromatography and tandem mass spectrometry (LC-MS/MS).

High-performance liquid chromatography and mass spectrometry (MS)

All liquid chromatography and MS experiments were carried out by the Southern Alberta Mass Spectrometry (SAMS) core facility at the University of Calgary, Canada. Analysis was performed on an Orbitrap Fusion Lumos Tribrid MS (Thermo Scientific) operated with Xcalibur (version 4.0.21.10) and coupled to a Thermo

Scientific Easy-nLC (nanoflow Liquid Chromatography) 1200 system. Tryptic peptides (2 µg) were loaded onto a C18 trap (75 µm × 2 cm; Acclaim PepMap 100, P/N 164946; ThermoScientific) at a flow rate of 2 µl/min of solvent A (0.1% formic acid and 3% acetonitrile in LC-MS grade water). Peptides were eluted using a 120 min gradient from 5 to 40% (5–28% in 105 min followed by an increase to 40% B in 15 min) of solvent B (0.1% formic acid in 80% LC-MS grade acetonitrile) at a flow rate of 0.3 µL/min and separated on a C18 analytical column (75 µm × 50 cm; PepMap RSLC C18; P/N ES803; Thermo Scientific). Peptides were then electrosprayed using 2.3 kV voltage into the ion transfer tube (300 °C) of the Orbitrap Lumos operating in positive mode. The Orbitrap first performed a full MS scan at a resolution of 120,000 FWHM to detect the precursor ion having a *m/z* between 375 and 1575 and a +2 to +7 charge. The Orbitrap AGC (Auto Gain Control) and the maximum injection time were set at 4 × 105 and 50 ms, respectively. The Orbitrap was operated using the top speed mode with a 3 s cycle time for precursor selection. The most intense precursor ions presenting a peptidic isotopic profile and having an intensity threshold of at least 5000 were isolated using the quadrupole and fragmented with HCD (30% collision energy) in the ion routing multipole. The fragment ions (MS^2) were analyzed in the ion trap at a rapid scan rate. The AGC and the maximum injection time were set at 1 × 104 and 35 ms, respectively, for the ion trap. Dynamic exclusion was enabled for 45 s to avoid of the acquisition of same precursor ion having a similar m/z (plus or minus 10 ppm).

Proteomic data and bioinformatics analysis

Spectral data were matched to peptide sequences in the murine UniProt protein database using the Andromeda algorithm[77] as implemented in the MaxQuant[33] software package v.1.6.10.23, at a peptide-spectrum match FDR of <0.01. Search parameters included a mass tolerance of 20 p.p.m. for the parent ion, 0.5 Da for the fragment ion, carbamidomethylation of cysteine residues (+57.021464 Da), variable N-terminal modification by acetylation (+42.010565 Da), and variable methionine oxidation (+15.994915 Da). N-terminal and lysine heavy (+34.063116 Da) and light (+28.031300 Da) dimethylation were defined as labels for relative quantification. The cleavage site specificity was set to Trypsin/P for the proteomics data, with up to two missed cleavages allowed. Significant outlier cutoff values were determined after log(2) transformation by boxplot-and-whiskers analysis using the BoxPlotR tool.[78]

Caspase-6 activity assay

Caspase-6 activity was measured by using Caspase-6 Colorimetric Assay Kit (K115, Biovision) according to the manufacturer's instruction. THP-1 macrophages were pre-treated with caspase-6 inhibitor Z-VEID-fmk 50 µM and stimulated with *Eh* (1:20, *Eh* to macrophage ratio) in absence or presence of inhibitor for 10 min. Cell lysates were prepared using the lysis buffer provided with the caspase-6 colorimetric assay kit. Absorbance were measured at different time points (2, 3, 4 h) at 405 nm.

mRNA expression analysis by real-time qPCR

Total RNA was extracted from snap-frozen tissue using Trizol reagent protocol (Invitrogen; Life Technologies, Burlington, ON) following manufacturer's instructions. The purity and yield of the RNA was detected by the ratio of absorbance at 260/280 nm (NanoDrop, Thermo Scientific). qScript cDNA synthesis kit was used to prepare cDNA. Rotor Gene 3000 real-time PCR system (Corbett Research) was used for mRNA expression analysis. Each reaction mixture contained 1:10 dilution of prepared cDNA, SYBR Green PCR Master Mix (Qiagen) and 2 µM of primers (F + R). Results were analyzed using the $2^{-\Delta\Delta CT}$ methods and expressed as fold changes relative to housekeeping genes. A complete list of the primer sequences and conditions used are listed in Supplementary Table S2.

Animals

C57BL/6 mice were obtained from Charles River. $Asc^{-/-}$ and $Nlrp3^{-/-}$ mice were obtained from Dr. D. Muruve (University of Calgary). ATG16L1 T316A variant mice on a C57BL/6 background were provided by Dr. H. Jijon (University of Calgary).

Mouse colonic loops with *Eh* infection

Short-term mouse closed colonic loop study was done as an *Eh* infection model following previously published protocol.[31] Concisely, mice were anesthetized and following laparotomy, the colon was externalized, and ligations was done with 3–0 black silk sutures (Ethicon, Somerville, NJ; Peterborough, ON, Canada) in the proximal colon (about 2 cm) carefully to retain the mesenteries, blood vessels, and nerves intact. Virulent log-phased WT *Eh* (1 × 106) in 100 µL PBS were injected into the colonic loop. The control group was injected with 100 µL PBS. After 3 h, tissues from the proximal colon were collected for RNA extraction, MPO assay and protein assay. For each experiment, $n = 6/7$ littermates (mice group matched by age) were used as controls and *Eh* inoculated group in three independent repeats of the experiment.

Ethics statement

The Health Sciences Animal Care Committee from the University of Calgary, have examined the animal care and treatment protocol (AC18-0218) and approved the experimental procedures proposed and certifies with the applicant that the care and treatment of animals used was in accordance with the principles outlined in the most recent policies on the "Guide to the Care and Use of Experimental Animals" by The Canadian Council on Animal Care.

Statistics

Experiments are representative of at least three independent experiments. Densitometry analysis was performed by Image Lab software. Statistical significance between two groups was done by Student's *t*-test and comparison between two or more groups were done by one-way ANOVA followed by *post hoc* Bonferroni test. GraphPad Prism8 was used for these statistical analysis and $P < 0.05$ was considered as significant. For the confocal image quantification, a minimum of seven images was used for each condition and with same brightness adjustment. Results were showed as the mean ± SEM. For colonic loop study $N =$ at least six mice were used for both control and *Eh* inoculation.

ACKNOWLEDGEMENTS

We like to generously thank Dr. D. Muruve for $Asc^{-/-}$ and $Nlrp3^{-/-}$ mice and Dr. H. Jijon for the ATG16L1 T316A variant mice.

AUTHOR CONTRIBUTIONS

S.B. and K.C. constructed the experimental design. K.C., F.M. and A.D. contributed reagents and methodical support. S.B. performed the majority of experiments and data analysis. F.M. contributed with mouse colonic loop study and in vitro cleavage experiments. S.B., A.D., and K.C. wrote the manuscript.

FUNDING

This work was funded by a Discovery Grant (RGPIN-2019-04136) from the Natural Sciences and Engineering Research Council of Canada and a project grant from the Canadian Institutes of Health Research (PJT-407276) awarded to K.C. The funders had no role in study design, data collection and analysis, decision to publish, or preparation of the manuscript.

ADDITIONAL INFORMATION

Supplementary information The online version contains supplementary material available at https://doi.org/10.1038/s41385-021-00408-4.

Competing interests: The authors declare no competing interests.

Publisher's note Springer Nature remains neutral with regard to jurisdictional claims in published maps and institutional affiliations.

REFERENCES

1. Haque, R., Huston, C., Huges, M., Houpt, E. & Petri, W. Jr Amoebiasis: review article. *N. Engl. J. Med.* **348**, 1565–1573 (2003).
2. Mortimer, L., Moreau, F., Cornick, S. & Chadee, K. The NLRP3 inflammasome is a pathogen sensor for invasive *Entamoeba histolytica* via activation of alpha5beta1 integrin at the macrophage-amebae intercellular junction. *PLoS Pathog.* **11**, e1004887 (2015).
3. Petri, W. A., Smith, R., Schlesinger, P., Murphy, C. & Ravdin, J. Isolation of the galactose-binding lectin that mediates the in vitro adherence of *Entamoeba histolytica*. *J. Clin. Investig.* **80**, 1238–1244 (1987).
4. Chadee, K., Petri, W., Innes, D. & Ravdin, J. Rat and human colonic mucins bind to and inhibit adherence lectin of *Entamoeba histolytica*. *J. Clin. Investig.* **80**, 1245–1254 (1987).
5. Moncada, D., Keller, K. & Chadee, K. *Entamoeba histolytica* cysteine proteinases disrupt the polymeric structure of colonic mucin and alter its protective function. *Infect. Immun.* **71**, 838–844 (2003).
6. Reed, S. L., Keene, W. E. & McKerrow, J. H. Thiol proteinase expression and pathogenicity of *Entamoeba histolytica*. *J. Clin. Microbiol.* **27**, 2772–2777 (1989).
7. Seguin, R., Mann, B. J., Keller, K. & Chadee, K. Identification of the galactose-adherence lectin epitopes of *Entamoeba histolytica* that stimulate tumor necrosis factor-alpha production by macrophages. *Proc. Natl Acad. Sci. USA* **92**, 12175–12179 (1995).
8. Shalini, S., Dorstyn, L., Dawar, S. & Kumar, S. Old, new and emerging functions of caspases. *Cell Death Differ.* **22**, 526–539 (2015).
9. Mortimer, L., Moreau, F., Cornick, S. & Chadee, K. Gal-lectin-dependent contact activates the inflammasome by invasive *Entamoeba histolytica*. *Mucosal Immunol.* **7**, 829–841 (2014).
10. Quach, J., Moreau, F., Sandall, C. & Chadee, K. *Entamoeba histolytica*-induced IL-1beta secretion is dependent on caspase-4 and gasdermin D. *Mucosal Immunol.* **12**, 323–339 (2019).
11. St-Pierre, J. et al. The macrophage cytoskeleton acts as a contact sensor upon interaction with *Entamoeba histolytica* to trigger IL-1beta secretion. *PLoS Pathog.* **13**, e1006592 (2017).
12. Seydel, K. B., Li, E., Zhang, Z. & Stanley, S. L. Jr Epithelial cell-initiated inflammation plays a crucial role in early tissue damage in amebic infection of human intestine. *Gastroenterology* **115**, 1446–1453 (1998).
13. Deretic, V., Saitoh, T. & Akira, S. Autophagy in infection, inflammation and immunity. *Nat. Rev. Immunol.* **13**, 722–737 (2013).
14. Yang, Z. & Klionsky, D. J. An overview of the molecular mechanism of autophagy. Autophagy in infection and immunity. 1–32 (Springer, 2009).
15. Saitoh, T. et al. Loss of the autophagy protein Atg16L1 enhances endotoxin-induced IL-1beta production. *Nature* **456**, 264–268 (2008).
16. Murthy, A. et al. A Crohn's disease variant in Atg16l1 enhances its degradation by caspase 3. *Nature* **506**, 456–462 (2014).
17. Lassen, K. G. et al. Atg16L1 T300A variant decreases selective autophagy resulting in altered cytokine signaling and decreased antibacterial defense. *Proc. Natl Acad. Sci. USA* **111**, 7741–7746 (2014).
18. Plantinga, T. S. et al. Crohn's disease-associated ATG16L1 polymorphism modulates pro-inflammatory cytokine responses selectively upon activation of NOD2. *Gut* **60**, 1229–1235 (2011).
19. Nakahira, K. et al. Autophagy proteins regulate innate immune responses by inhibiting the release of mitochondrial DNA mediated by the NALP3 inflammasome. *Nat. Immunol.* **12**, 222–230 (2011).
20. Shibutani, S. T., Saitoh, T., Nowag, H., Munz, C. & Yoshimori, T. Autophagy and autophagy-related proteins in the immune system. *Nat. Immunol.* **16**, 1014–1024 (2015).
21. Mizushima, N., Levine, B., Cuervo, A. M. & Klionsky, D. J. Autophagy fights disease through cellular self-digestion. *Nature* **451**, 1069–1075 (2008).
22. Levine, B. & Deretic, V. Unveiling the roles of autophagy in innate and adaptive immunity. *Nat. Rev. Immunol.* **7**, 767–777 (2007).
23. Fujita, N. et al. The Atg16L complex specifies the site of LC3 lipidation for membrane biogenesis in autophagy. *Mol. Biol. Cell* **19**, 2092–2100 (2008).
24. Mizushima, N. et al. Mouse Apg16L, a novel WD-repeat protein, targets to the autophagic isolation membrane with the Apg12-Apg5 conjugate. *J. Cell Sci.* **116**, 1679–1688 (2003).
25. Jacobs, T., Bruchhaus, I., Dandekar, T., Tannich, E. & Leippe, M. Isolation and molecular characterization of a surface-bound proteinase of *Entamoeba histolytica*. *Mol. Microbiol* **27**, 269–276 (1998).
26. Melendez-Lopez, S. G. et al. Use of recombinant *Entamoeba histolytica* cysteine proteinase 1 to identify a potent inhibitor of amebic invasion in a human colonic model. *Eukaryot. Cell* **6**, 1130–1136 (2007).
27. Tillack, M. et al. The *Entamoeba histolytica* genome: primary structure and expression of proteolytic enzymes. *BMC Genomics* **8**, 170 (2007).
28. Klaiman, G., Champagne, N. & LeBlanc, A. C. Self-activation of Caspase-6 in vitro and in vivo: Caspase-6 activation does not induce cell death in HEK293T cells. *Biochim Biophys. Acta* **1793**, 592–601 (2009).
29. Wang, X. J. et al. Crystal structures of human caspase 6 reveal a new mechanism for intramolecular cleavage self-activation. *EMBO Rep.* **11**, 841–847 (2010).
30. Slee, E. A. et al. Ordering the cytochrome c-initiated caspase cascade: hierarchical activation of caspases-2, -3, -6, -7, -8, and -10 in a caspase-9-dependent manner. *J. Cell Biol.* **144**, 281–292 (1999).
31. Kissoon-Singh, V., Moreau, F., Trusevych, E. & Chadee, K. *Entamoeba histolytica* exacerbates epithelial tight Junction permeability and proinflammatory responses in Muc2$^{-/-}$ mice. *Am. J. Pathol.* **182**, 852–865 (2013).
32. McStay, G. P., Salvesen, G. S. & Green, D. R. Overlapping cleavage motif selectivity of caspases: implications for analysis of apoptotic pathways. *Cell Death Differ.* **15**, 322–331 (2008).
33. Cox, J. & Mann, M. MaxQuant enables high peptide identification rates, individualized ppb-range mass accuracies and proteome-wide protein quantification. *Nat. Biotechnol.* **26**, 1367–1372 (2008).
34. Zhou, Y. et al. Metascape provides a biologist-oriented resource for the analysis of systems-level datasets. *Nat. Commun.* **10**, 1–10 (2019).
35. Damian, S. et al. Mering Christian von. STRING v11: protein–protein association networks with increased coverage, supporting functional discovery in genome-wide experimental datasets. *Nucleic Acids Res.* **47**, D607–D613 (2018).
36. Komatsu, M. et al. Impairment of starvation-induced and constitutive autophagy in Atg7-deficient mice. *J. Cell Biol.* **169**, 425–434 (2005).
37. Furuta, N. & Amano, A. SNARE mediates autophagosome–lysosome fusion. *J. Oral. Biosci.* **54**, 83–85 (2012).
38. Chen, F., Amgalan, D., Kitsis, R. N., Pessin, J. E. & Feng, D. ATG16L1 autophagy pathway regulates BAX protein levels and programmed cell death. *J. Biol. Chem.* **295**, 15045–15053 (2020).
39. Dall, E. & Brandstetter, H. Structure and function of legumain in health and disease. *Biochimie* **122**, 126–150 (2016).
40. Sepulveda, F. E. et al. Critical role for asparagine endopeptidase in endocytic Toll-like receptor signaling in dendritic cells. *Immunity* **31**, 737–748 (2009).
41. Anderson, B. M. et al. N-Terminomics/TAILS Profiling of Macrophages after Chemical Inhibition of Legumain. *Biochemistry* **59**, 329–340 (2019).
42. Crowe, L. A. N. et al. S100A8 & S100A9: Alarmin mediated inflammation in tendinopathy. *Sci. Rep.* **6**(1), 1463 (2019).
43. Gruden-Movsesijan, A. & Milosavljevic, L. S. The involvement of the macrophage mannose receptor in the innate immune response to infection with parasite *Trichinella spiralis*. *Vet. Immunol. Immunopathol.* **109**, 57–67 (2006).
44. Pineda, E. & Perdomo, D. *Entamoeba histolytica* under oxidative stress: what countermeasure mechanisms are in place? *Cells* **6**, 44 (2017).
45. Nakada-Tsukui, K. & Nozaki, T. Immune response of amebiasis and immune evasion by *Entamoeba histolytica*. *Front Immunol.* **7**, 175 (2016).
46. Glick, D., Barth, S. & Macleod, K. F. Autophagy: cellular and molecular mechanisms. *J. Pathol.* **221**, 3–12 (2010).
47. Zhou, R., Yazdi, A. S., Menu, P. & Tschopp, J. A role for mitochondria in NLRP3 inflammasome activation. *Nature* **469**, 221–225 (2011).
48. Lupfer, C. et al. Receptor interacting protein kinase 2-mediated mitophagy regulates inflammasome activation during virus infection. *Nat. Immunol.* **14**, 480–488 (2013).
49. Wang, C. et al. Atg16L1 deficiency confers protection from uropathogenic *Escherichia coli* infection in vivo. *Proc. Natl Acad. Sci. USA* **109**, 11008–11013 (2012).
50. Cadwell, K. et al. A common role for Atg16L1, Atg5, and Atg7 in small intestinal Paneth cells and Crohn disease. *Autophagy* **5**, 250–252 (2009).
51. Plantinga, T. S. et al. Crohn's disease-associated ATG16L1 polymorphism modulates pro-inflammatory cytokine responses selectively upon activation of NOD2. *Gut* **60**, 1229–1235 (2011).
52. Conway, K. L. et al. Atg16l1 is required for autophagy in intestinal epithelial cells and protection of mice from *Salmonella* infection. *Gastroenterology* **145**, 1347–1357 (2013).
53. Trentesaux, C. et al. Essential role for autophagy protein ATG7 in the maintenance of intestinal stem cell integrity. *Proc. Natl Acad. Sci. USA* **117**, 11136–11146 (2020).

54. Verma, A. K., Verma, R., Ahuja, V. & Paul, J. Real-time analysis of gut flora in *Entamoeba histolytica* infected patients of Northern India. *BMC Microbiol* **12**, 183 (2012).
55. Morton, E. R. et al. Variation in rural African gut microbiota is strongly correlated with colonization by *Entamoeba* and subsistence. *PLoS Genet* **11**, e1005658 (2015).
56. Gilchrist, C. A. et al. Role of the gut microbiota of children in diarrhea due to the protozoan parasite *Entamoeba histolytica*. *J. Infect. Dis.* **213**, 1579–1585 (2016).
57. Ravikumar, B., Imarisio, S., Sarkar, S., O'Kane, C. J. & Rubinsztein, D. C. Rab5 modulates aggregation and toxicity of mutant huntingtin through macroautophagy in cell and fly models of Huntington disease. *J. Cell Sci.* **121**, 1649–1660 (2008).
58. Szatmári, Z. & Sass, M. The autophagic roles of Rab small GTPases and their upstream regulators: a review. *Autophagy* **10**, 1154–1166 (2014).
59. Ao, X., Zou, L. & Wu, Y. Regulation of autophagy by the Rab GTPase network. *Cell Death Differ.* **21**, 348–358 (2014).
60. Amaya, C., Fader, C. M. & Colombo, M. I. Autophagy and proteins involved in vesicular trafficking. *FEBS Lett.* **589**, 3343–3353 (2015).
61. Pilli, M. et al. TBK-1 promotes autophagy-mediated antimicrobial defense by controlling autophagosome maturation. *Immunity* **37**, 223–234 (2012).
62. Furuta, N., Fujita, N., Noda, T., Yoshimori, T. & Amano, A. Combinational soluble N-ethylmaleimide-sensitive factor attachment protein receptor proteins VAMP8 and Vti1b mediate fusion of antimicrobial and canonical autophagosomes with lysosomes. *Mol. Biol. Cell* **21**, 1001–1010 (2010).
63. Chen, K. et al. Toll-interacting protein deficiency promotes neurodegeneration via impeding autophagy completion in high-fat diet-fed ApoE$^{-/-}$ mouse model. *Brain, Behav. Immun.* **59**, 200–210 (2017).
64. He, C. et al. A novel *Entamoeba histolytica* cysteine proteinase, EhCP4, is key for invasive amebiasis and a therapeutic target. *J. Biol. Chem.* **285**, 18516–18527 (2010).
65. Begum, S., Moreau, F., Leon Coria, A. & Chadee, K. *Entamoeba histolytica* stimulates the alarmin molecule HMGB1 from macrophages to amplify innate host defenses. *Mucosal Immunol.* **13**, 344–356 (2020).
66. McIlwain, D. R., Berger, T. & Mak, T. W. Caspase functions in cell death and disease. *Cold Spring Harb. Perspect. Biol.* **5**, a008656 (2013).
67. Bartel, A., Gohler, A., Hopf, V. & Breitbach, K. Caspase-6 mediates resistance against *Burkholderia pseudomallei* infection and influences the expression of detrimental cytokines. *PLoS One* **12**, e0180203 (2017).
68. Kobayashi, H. et al. Neutrophils activate alveolar macrophages by producing caspase-6-mediated cleavage of IL-1 receptor-associated kinase-M. *J. Immunol.* **186**, 403–410 (2011).
69. Ladha, S. et al. Constitutive ablation of caspase-6 reduces the inflammatory response and behavioural changes caused by peripheral pro-inflammatory stimuli. *Cell Death Disco.* **4**, 40 (2018).
70. Sharma, A., Kaur, S., Duseja, A. & Changotra, H. The autophagy gene ATG16L1 (T300A) variant is associated with the risk and progression of HBV infection. *Infect Genet Evol*, **84**, 104404 (2020).
71. Guo, X. et al. Leptin signaling in intestinal epithelium mediates resistance to enteric infection by *Entamoeba histolytica*. *Mucosal Immunol.* **4**, 294–303 (2011).
72. Duggal, P. et al. A mutation in the leptin receptor is associated with *Entamoeba histolytica* infection in children. *J. Clin. Investig.* **121**, 1191–1198 (2011).
73. Graham, R. K., Ehrnhoefer, D. E. & Hayden, M. R. Caspase-6 and neurodegeneration. *Trends Neurosci.* **34**, 646–656 (2011).
74. Dagbay, K. B. & Hardy, J. A. Multiple proteolytic events in caspase-6 self-activation impact conformations of discrete structural regions. *Proc. Natl Acad. Sci. USA* **114**, E7977–e7986 (2017).
75. Diamond, L. S., Harlow, D. R. & Cunnick, C. C. A new medium for the axenic cultivation of *Entamoeba histolytica* and other *Entamoeba*. *Trans. R. Soc. Trop. Med. Hyg.* **72**, 431–432 (1978).
76. Hou, Y., Mortimer, L. & Chadee, K. *Entamoeba histolytica* cysteine proteinase 5 binds integrin on colonic cells and stimulates NFkappaB-mediated pro-inflammatory responses. *J. Biol. Chem.* **285**, 35497–35504 (2010).
77. Cox, J. et al. Andromeda: a peptide search engine integrated into the MaxQuant environment. *J. Proteome Res.* **10**, 1794–1805 (2011).
78. Spitzer, M., Wildenhain, J., Rappsilber, J. & Tyers, M. BoxPlotR: a web tool for generation of box plots. *Nat. Methods* **11**, 121 (2014).